Research paper

Late Miocene provenance change on the eastern margin of the Yinggehai-Song Hong Basin, South China Sea: Evidence from U−Pb dating and Hf isotope analyses of detrital zircons

Ce Wang [a, b], Xinquan Liang [a, *], Yuhong Xie [c], Chuanxin Tong [c], Jianxiang Pei [c], Yun Zhou [a, b], Ying Jiang [a, b], Jiangang Fu [a, b], Shunv Wen [d]

[a] State Key Laboratory of Isotope Geochemistry, Guangzhou Institute of Geochemistry, Chinese Academy of Sciences, Guangzhou 510640, China
[b] University of Chinese Academy of Sciences, Beijing 100049, China
[c] China National Offshore Oil Corporation Ltd., Zhanjiang 524057, China
[d] School of Earth Science, Guilin University of Technology, Guilin 541004, China

ARTICLE INFO

ABSTRACT

Understanding the provenance of the reservoir in a sedimentary basin is of great importance in hydrocarbon exploration and production. The Yinggehai-Song Hong Basin is one of the most important Cenozoic petroliferous basins in the South China Sea. To better understand the provenance characteristics of the Upper Miocene Huangliu Formation (Tortonian-Messinian) on the eastern margin of the basin and test the influence of uplift of the Tibetan Plateau in the South China Sea, 172 single zircons from two sandstone samples in the Lingtou gas field were dated by U−Pb chronometer, and 54 of these grains were spot analyzed for Hf isotopes. The results indicate that the upper member of the Huangliu Formation in this gas field shows two major peaks of U−Pb ages at ca. 250 Ma and ca. 432 Ma, along with four subordinate peaks at ca. 757 Ma, ca. 1926 Ma, ca. 2529 Ma and ca. 2775 Ma. The initial Hf isotope ratios [$\varepsilon_{Hf}(t)$] of these zircons are negative to positive for each age group, suggesting that existing crustal materials were mixing with new mantle melts in some magmatic episodes. In contrast, the lower member of the Huangliu Formation show two major age peaks at ca. 98 Ma and 248 Ma, with a subordinate peak at ca. 1453 Ma. The $\varepsilon_{Hf}(t)$ values are concentrated between −11.6 and −3.4, revealing that they were derived from older crust. Comparing with the source characteristics of tectonic units surrounding the basin, the source of the upper member in the gas field was mainly from the southern Yangtze Block, whereas the lower member was derived from the Hainan Uplift. Together with the change of climate and sedimentation rate after 10 Ma on the northern margin of the South China Sea, we attribute the provenance change to the uplift of the Tibetan Plateau at the same time.

1. Introduction

Studies on the provenance of a reservoir and its transport routes are critical to establish its tectonic evolution in a sedimentary basin (Morton et al., 2001; Tsikouras et al., 2011). Uncertainties in the provenance and distribution of the reservoir may contribute to operational risks in drilling. The Upper Miocene Huangliu Formation is an important hydrocarbon exploration target in the Yinggehai-Song Hong (Y-SH) Basin, South China Sea. During the last

decade, much attention has been paid to the provenance of the deep marine sedimentary rocks of the Huangliu Formation due to its huge gas potential and commercial value. Several published research papers focused on the petrography, sequence stratigraphy, geochemistry, heavy mineral analysis, and whole-rock isotopes and geochronology (e.g. Gong et al., 1997; Wu, 1997; Huang et al., 2003; Yan et al., 2007; Xie, 2009; Lei et al., 2011; Yan et al., 2011; Wang et al., 2014), which greatly enhanced our understanding of the distribution of reservoir in the basin. Yan et al. (2011) used detrital zircon geochronology of the eastern slope of the basin (Fig. 1B) to show that two major age peaks at 110−90 Ma and 275−225 Ma, suggest the source was derived from Hainan Island. Wang et al. (2014) used the same methods to constrain the provenance of the
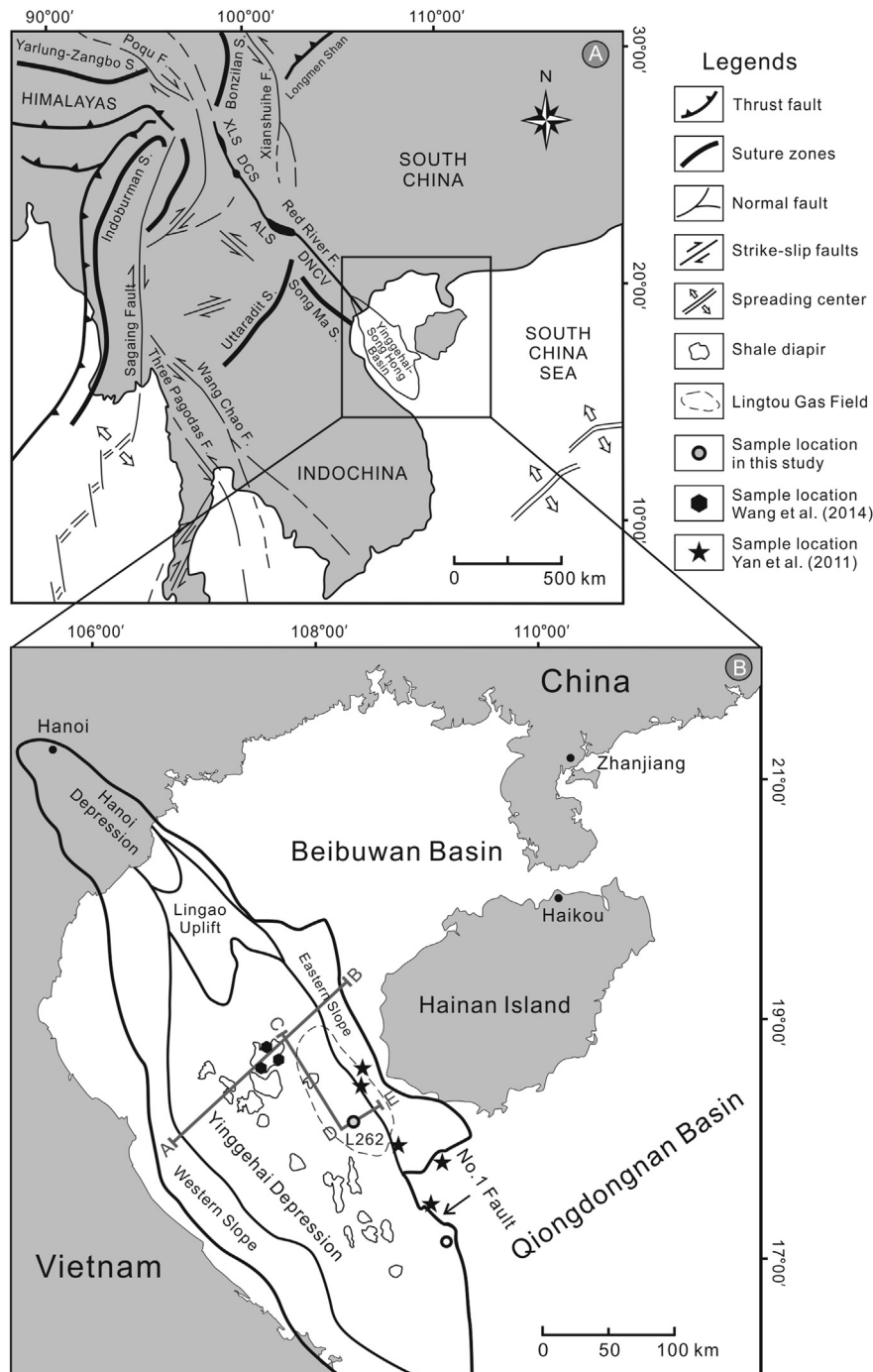
Figure 1. Geologic sketch map of the Yinggehai-Song Hong Basin, (A) Modified after Tapponnier et al. (1990), Leloup et al. (1995), Gilley et al. (2003) and Zhu et al. (2009); (B) Modified after Huang et al. (2005) and Lei et al. (2011).

sedimentary rocks in the Dongfang gas field in the central Y-SH Basin. The authors argued that the detritus in the Dongfang gas field was derived from multiple sources since the Late Miocene. Conventional heavy minerals, seismic profiles and sedimentary facies data suggest that the sediments of the Huangliu Formation in the Lingtou gas field are also derived from Hainan Island (Gong et al., 1997; Xie, 2009). However, the conclusion is skeptical because the basin is located in structurally complex regions with multiple source areas (e.g. Indochina and Yangtze blocks) (Wang et al., 2014), and lacks precise geochronologic and isotopic data. Therefore, the provenance of the sandstones in the Lingtou gas field

remains unclear. Although conventional methods of determining provenance appear to reach their limits and cannot meet the needs of further hydrocarbon exploration, U–Pb ages add the time dimension to the provenance analysis (Beltrán-Triviño et al., 2013). U–Pb dating of detrital zircon is one of the most widely used methods in provenance studies, especially combined with Hf isotopes (e.g. Griffin et al., 2004; Meinhold et al., 2008; Wu et al., 2010; Zhao et al., 2013).

This study uses combined U–Pb and Lu–Hf isotope analyses of detrital zircons from marine core samples to constrain sedimentary provenance of the Huangliu Formation in the Lingtou gas field,

eastern margin of the Y-SH Basin. The main purposes of the study are (a) to understand zircon age compositions of the Upper Miocene Huangliu Formation in the gas field; (b) to determine the sedimentary provenance; and (c) to discuss provenance changes and their tectonic implications.

2. Geological setting

The NNW–SSE trending Y-SH Basin, located and surrounded by the Hainan Island to the east, the South China Block to the south and the Indochina Block to the west (Fig. 1), is a Cenozoic pull-apart basin. The basin was developed on the northern margin of the South China Sea continental shelf, and the formation was generally considered to be related to the southeastward strike-slip deformation and clockwise rotation of the Indochina Block as a result of the collision and indentation of India into Asia (Fig. 1A) (Molnar and Tapponnier, 1975; Tapponnier et al., 1986; Guo et al., 2001; Sun et al., 2003; Yan et al., 2011). The basin is bordered on the north

and east by the Beibuwan and Qiongdongnan basins, respectively (Fig. 1B).

Up to now, a number of commercial gas fields have been found in young, shallow reservoirs in the basin. The stratigraphic units related to hydrocarbon generation and accumulation are divided into: the Lingtou Formation (Eocene); Yacheng and Lingshui formations (Middle and Upper Oligocene, respectively); the Sanya, Meishan, and Huangliu formations (Miocene) and the Yinggehai Formation (Pliocene), which are covered by Quaternary sediments and underlain by pre-Paleogene strata (Fig. 2) (Gong et al., 1997; Geng et al., 1998; Gong and Li, 2004). The basin is characterized by its large volumes, subsidence rates, overpressures, and diapirs which widely developed in the central Yinggehai Depression (Zhang et al., 1996; Luo et al., 2003; Huang et al., 2009). These diapirs, in an en echelon arrangement, and varying in shape and size, have been recognized by their great significance in hydrocarbon exploration (Xie et al., 2001; Wang and Huang, 2008; Huang et al., 2009; Lei et al., 2011) (Fig. 1B). The basin contains up to 17 km thick

Epoch		Strata	Member	Abbreviation	Age (Ma)	Maximum thickness (m)	Lithology	Depositional environment
Quaternary		Ledong		Q		1250		Littoral
Neogene	Pliocene	Yinggehai	I / II	N_2	T20 — 1.9 / T30 — 5.5	2200		Littoral to Bathyal
	Miocene	Huangliu	I / II	N_1^3	T40 — 10.5	780		Littoral to Neritic
		Meishan	I / II	N_1^2	T50 — 16.5	1750		Littoral to Neritic
		Sanya	I / II	N_1^1	T60 — 21.0	2950		Littoral to Neritic
Paleogene	Oligocene	Lingshui	I / II / III	E_3^2	T70 — 30.0	Undrilled		Littoral to Neritic
		Yacheng	I / II / III	E_3^1	T80 — 37.0			Coastal plain to Neritic
	Eocene	Lingtou		E_2	T100 — 49.5			Lacustrine
Pre-Paleogene Basement								

Conglomerate   Sandstone   Mudstone   Silty mudstone   Contactolite   Unconformity

Figure 2. Regional stratigraphic column of the Y-SH Basin, modified after Gong et al. (1997), Huang et al. (2003) and Xie (2009).

of Paleogene to Quaternary sedimentary rocks (Gong et al., 1997; Yan et al., 2011). The infill sedimentary rocks in the central Ying-gehai depression is composed by lacustrine, littoral and neritic to littoral and bathyal clastic deposits. The depositional facies of the Huangliu Formation (T40−T30) are shown in Figure 3.

3. Sampling and analytical methods

3.1. Sampling

Two sedimentary rock samples (L262-1 and L262-2) were collected from the core library of CNOOC Ltd., Zhanjiang, China.

Sample L262-1 was collected from the upper member of the Huangliu Formation (8.2−5.5 Ma) that consists mainly of fine sandstones, siltstones and mudstones at a depth of 2535 m. Sample L262-2 was selected from the lower member of the Huangliu For-mation (10.5−8.2 Ma) that is composed mainly of gray green sandstones and mudstones at a depth of 2740 m (Figs. 3 and 4). Both samples were from the "L262 well" which is located in the Lingtou gas field, eastern margin of the Yinggehai Depression (GPS: N 18°22′10″, E 108°22′30″) (Figs. 1B and 4).

3.2. Zircon U−Pb isotopic analysis by LA-ICP-MS

Detrital zircon U−Pb dating was performed on polished grain mounts by laser ablation-inductively coupled plasma-mass spec-trometry (LA-ICP-MS). Zircons from the two samples were sepa-rated using heavy liquids and a Frantz magnetic separator, following purification by hand sorting. Zircon grains were mounted in epoxy and polished down to near half sections to expose internal structures. Approximately 300 zircon grains were handpicked from each sample.

Cathodoluminescence (CL) imaging of zircon grains was carried out using a Gatan Mono CL detector attached to an Electron Microprobe (JSM6510, Japan) at Beijing GeoAnalysis Co., Ltd., to identify the internal structures of the grains and to select target sites for laser ablation analyses. Zircons were dated using a LA-ICP-MS hosted at the State Key Laboratory of Isotopic Geochemistry, Guangzhou Institute of Geochemistry, Chinese Academy of Sciences (GIG-CAS). Sample mounts were placed in the two-volume sample cell flushed with Ar and He. Laser ablation was operated at a con-stant energy of 80 mJ and at 8 Hz, with a spot diameter of 33 μm. The ablated material was carried by the He gas to the Aglient 7500a ICP-MS. Element corrections were made for mass bias drift, which was evaluated by reference to standard glass NIST SRM 610. The

Temora was used as the age standard ($^{206}Pb/^{238}U = 416.8$ Ma) (Black et al., 2003). Details of analytical procedure, precision and accuracy are similar to those of Jackson et al. (2004), Yuan et al. (2004) and Liu et al. (2010).

The $^{206}Pb/^{238}U$ ages <1000 Ma are used, whereas $^{207}Pb/^{206}Pb$ ages were selected if the $^{206}Pb/^{238}U$ ages were older than 1000 Ma. For statistical purposes, ages which display more than ±10% discordance were rejected in this study. Isotopic ratios of U−Th−Pb were calculated using ICPMSDataCal (Version 7.2) (Liu et al., 2008, 2010). Common Pb was corrected by ComPbCorr#3_151 using the method of Andersen (2002). The age calculation and concordia plots were made using ISOPLOT (Version 3.0) (Ludwig, 2003). To show accuracy and analytical precision, data points are displayed on concordia plots as filled error ellipses, with all errors reported at the 1 Sigma confidence level.

3.3. Zircon Hf isotopic analysis by LA-MC-ICP-MS

In situ zircon Lu−Hf isotopic analysis was carried out on a Neptune Plus multi-collector ICP-MS equipped with a RESOlution M-50 laser-ablation system at the State Key Laboratory of Isotopic Geochemistry, GIG-CAS. The Lu−Hf isotopic measurements were made on the same spots that were previously analyzed for U−Pb ages. The laser pa-rameters were as follows: spot size, 45 μm; repetition rate, 8 Hz; energy, 80 mJ. Helium was used as a carrier gas and a small flow of nitrogen was added in the gas line to enhance the sample signal. A normal single spot analysis consists of 30 s gas blank collection and 30 s laser ablation. The integration time was 0.131 s and about 200 cycles of data were collected. ^{173}Yb and ^{175}Lu were used to correct the isobaric interference of ^{176}Yb and ^{176}Lu on ^{176}Hf. The $^{176}Hf/^{177}Hf$ was normalized to $^{179}Hf/^{177}Hf$ 0.7325 using an exponential law for mass bias correction. Penglai sample was used as the reference standard (Li et al., 2010). The analytical procedures were the same as those described by Wu et al. (2006) and Yuan et al. (2008).

The initial Hf isotope ratios are denoted as $\varepsilon_{Hf}(t)$ values that were calculated with the Chondritic Uniform Reservoir (CHUR) at the time of zircon crystallization, and the present-day $^{176}Hf/^{177}Hf$ and $^{176}Lu/^{177}Hf$ ratios of chondrite and depleted mantle of 0.28277 and 0.0332, 0.28325 and 0.0384, respectively (Blichert-Toft and Albarède, 1997). Initial $^{176}Hf/^{177}Hf$ values were calculated based on ^{176}Lu decay constant of 1.865×10^{-11} year^{-1} (Scherer et al., 2001). The single-stage model Hf ages (T$_{DM1}$) were computed with reference to the depleted mantle with a present-day $^{176}Lu/^{177}Hf$ ratio of 0.28325 and a $^{176}Lu/^{177}Hf$ ratio of 0.0384 (Griffin et al., 2000). Two-stage model Hf ages (T$_{DM2}$) were
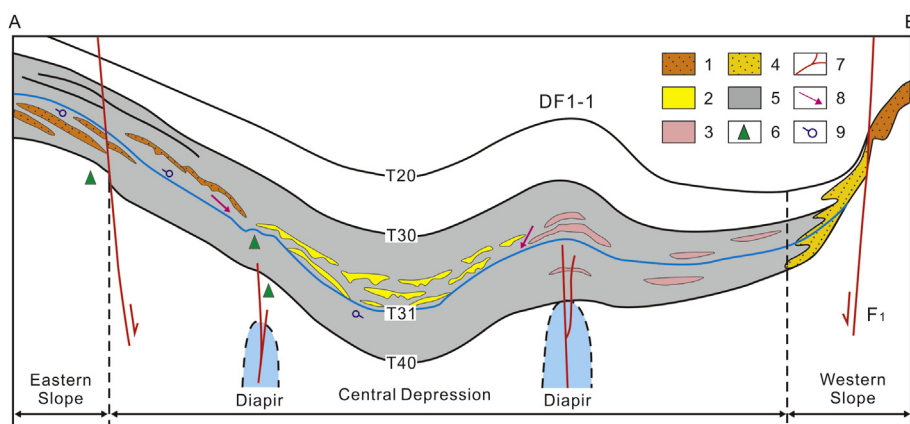
Figure 3. Section of depositional facies of the Huangliu Formation (T40−T30) in the Y-SH Basin. Position of the section is shown in Figure. 1B, modified after Zhang et al. (2013). Legend: 1- Delta; 2- Submarine fan; 3- Neritic beach and bar; 4- Seashore; 5- Neritic; 6- Tectonic slope break; 7- Fault; 8- Downlap; 9- Truncation. T30−T31: the upper member of the Huangliu Formation; T31−T40: the lower member of the Huangliu Formation.
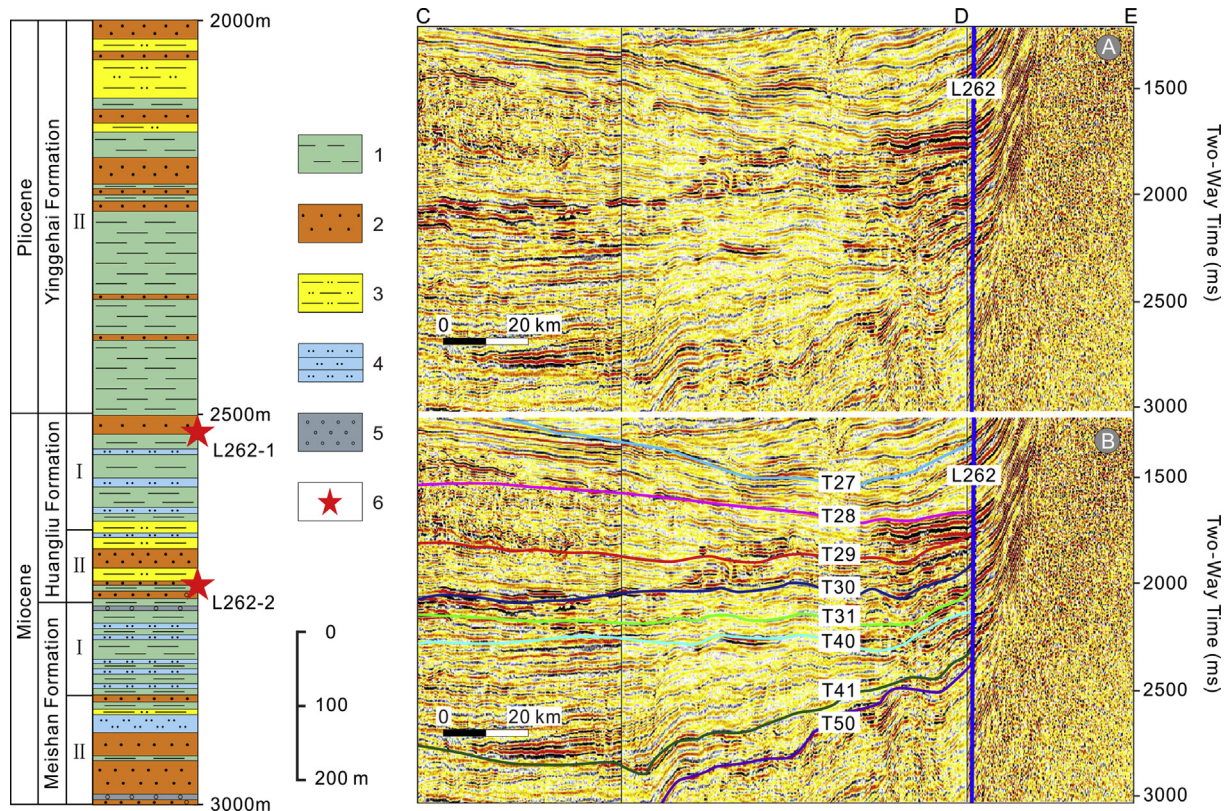
Figure 4. Measured Miocene to Pliocene sequences of L262 drill core on the eastern margin of the Y-SH Basin and giving positions of investigated sandstone samples (Left). Un-interpreted (a) and interpreted (b) seismic profile shows the conformable contact between the upper and lower members of the Huangliu Formation (T30–T31 and T31–T40, respectively) (Right). Legend: 1-mudstone; 2-sandstone; 3-argillaceous siltstone; 4-siltstone; 5-conglomerate.
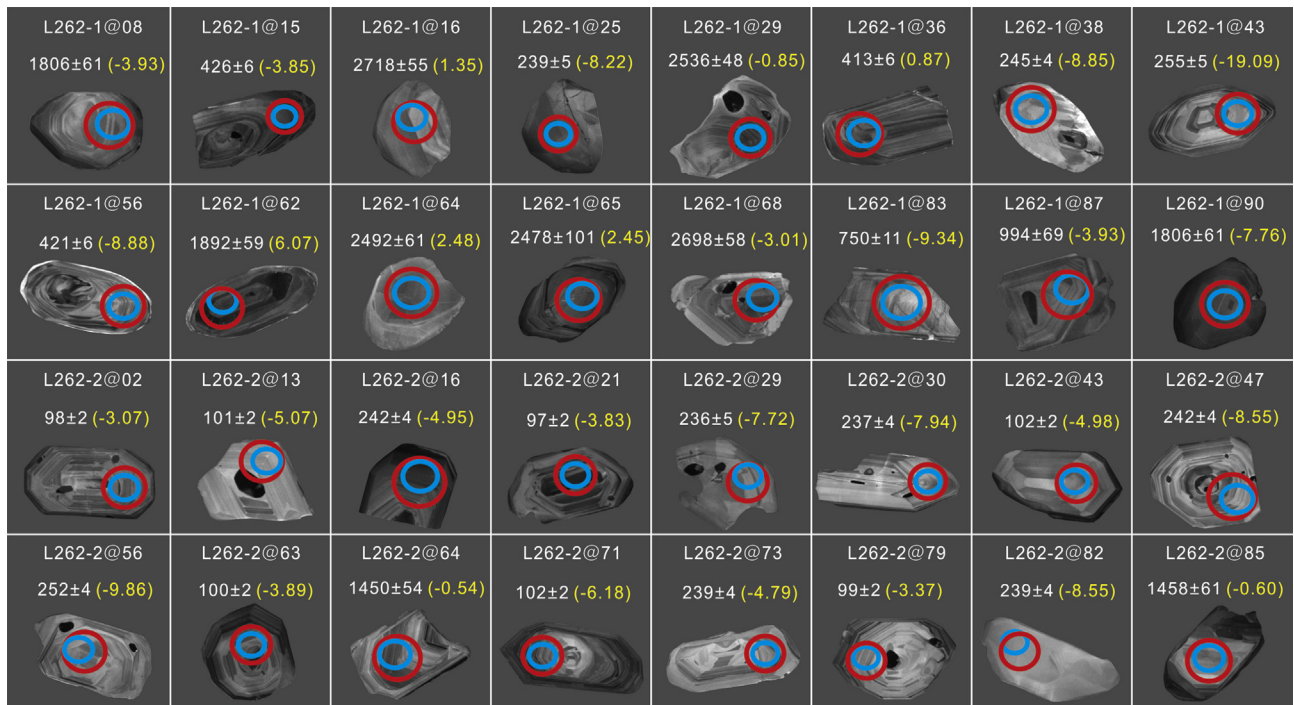
Figure 5. CL images of representative detrital zircons analyzed for the U−Pb ages and Lu−Hf isotopes. The large and small circles denote the LA-(MC)-ICP-MS analytical spots for the U−Pb ages and Lu−Hf isotopes, respectively. Numbers near the circles are U−Pb (^{207}Pb/^{206}Pb ages are selected for zircons older than 1000 Ma and ^{206}Pb/^{238}U ages for zircons less than 1000 Ma), with the $\varepsilon_{Hf}(t)$ values (within parentheses). The blue and red circles are 33 μm and 45 μm in diameter, respectively. (For interpretation of the references to color in this figure legend, the reader is referred to the web version of this article.)

computed using a ^{176}Lu/^{177}Hf value of 0.015 for average continental crust (Griffin et al., 2002). During the analyses, the ^{176}Hf/^{177}Hf and ^{176}Lu/^{177}Hf ratios of standard zircon (Penglai) were 0.282907 ± 0.000016 (2σ, $n = 20$) and 0.000303, respectively. These values agree with the recommended ^{176}Hf/^{177}Hf values for Penglai (0.282906 ± 0.000016, 2σ, $n = 117$) (Li et al., 2010).

4. Results

CL images of representative zircons from the studied samples together with spot ages and $\varepsilon_{Hf}(t)$ values are shown in Figure 5. The U–Pb age data are shown on concordia plots and relative age probability diagrams (Fig. 6), and are presented in detail in Table 1. The Hf isotope results are given in Table 2 and illustrated in Figures 7 and 8.

4.1. Zircon U–Pb ages

4.1.1. Sample L262-1 (the upper member of the Huangliu Formation)

More than 300 zircon grains were separated from sample L262-1 which was collected from the upper member of the Huangliu Formation in the Lingtou gas field. The zircon grains are colorless and transparent, and show a wide range of shapes from prismatic crystals to oval grains with mostly rounded corners (Fig. 5), suggestive of a long transport of some zircons before deposition, or multi-cycle deposition. In addition, some zircon grains are incomplete, and they may have been damaged during transport. The zircon grains reach up to 300 μm long, but are mainly in the range of 90–110 μm. Most grains show oscillatory growth zoning under CL (Fig. 5) and have high Th/U values (>0.4). All of these features indicate that the majority of the analyzed zircons are of a magmatic origin (Wu and Zheng, 2004).

Of the 90 analyses conducted on 90 zircons for this sample, 87 analyses are concordant within error (Fig. 6A). The measured ^{206}Pb/^{238}U (<1000 Ma) and ^{207}Pb/^{206}Pb (>1000 Ma) ages range from 3169 to 83 Ma. There are two major age peaks at ca. 250 Ma and ca. 432 Ma, along with a number of subordinate age peaks at ca. 757 Ma, ca. 1926 Ma, ca. 2529 Ma and ca. 2775 Ma.

4.1.2. Sample L262-2 (the lower member of the Huangliu Formation)

Over 300 colorless zircon grains were separated from sample L262-2 which was collected from the lower member of the Huangliu Formation in the Lingtou gas field. Most of the zircon grains are angular or subangular (Fig. 5) and appear to have retained their euhedral crystal shapes, implying short transport before deposition. The grains reach up to 200 μm long, but mainly range from 80 to 100 μm. Most of the grains show oscillatory growth zoning in CL images (Fig. 5), and have high Th/U ratios (>0.4), indicating that the majority of the analyzed zircons are of a magmatic origin (Wu and Zheng, 2004).

Of the 85 analyses conducted on 85 zircons for this sample, all of the analyses are concordant within error (Fig. 6B). The measured ^{206}Pb/^{238}U (<1000 Ma) and ^{207}Pb/^{206}Pb (>1000 Ma) ages range from 1457 to 93 Ma. There are two major age peaks at ca. 98 Ma and ca. 241 Ma, with a subordinate age peak at ca. 1453 Ma.

4.2. In situ zircon Hf isotopes

LA-MC-ICP-MS zircon Hf isotope measurements were performed following LA-ICP-MS U–Pb dating. Fifty-four dated zircon grains from the two samples (L262-1 and L262-2) were selected for in situ Hf isotope analyses. The sequence of analyses allowed the U–Pb ages and Hf isotopes to be done on the same spots as shown in Figure 5.

Twenty-nine spots were made on 29 zircon grains from sample L262-1. The results show a broad range of the initial ^{176}Hf/^{177}Hf ratios from 0.2810 to 0.2825, with $\varepsilon_{Hf}(t)$ values of −27.9 to 6.1
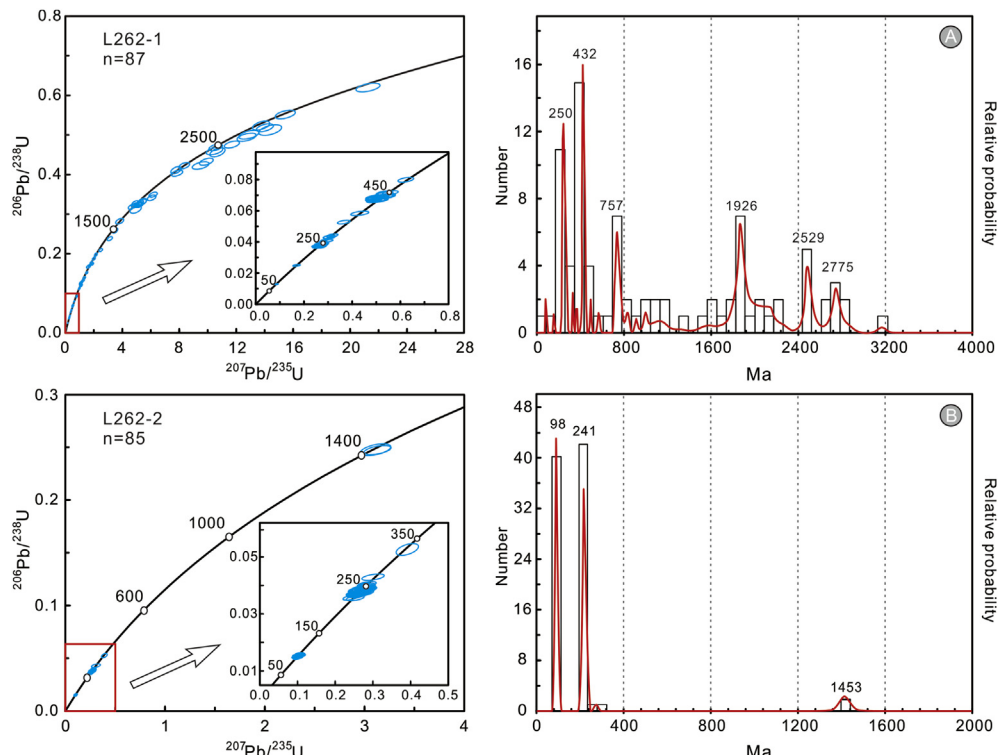
Figure 6. U–Pb Concordia and histogram diagram of detrital zircons for the two samples from the eastern margin of the Y-SH Basin. Data-point error ellipses are 1 sigma.

Table 1

LA-ICP-MS U—Pb dating results of the detrital zircons from the eastern margin of the Y-SH Basin. Ages which have more than ±10% discordance are shown by bold font.

Grain no.	Element (ppm)		Th/U	Ratios						Age (Ma)						Discordant text
	Th	U		$^{207}Pb/^{206}Pb$	1σ	$^{207}Pb/^{235}U$	1σ	$^{206}Pb/^{238}U$	1σ	$^{207}Pb/^{206}Pb$	1σ	$^{207}Pb/^{235}U$	1σ	$^{206}Pb/^{238}U$	1σ	
Sample: L262-1																
L262-1@01	101.82	68.43	1.49	0.07085	0.00392	1.62284	0.08888	0.16751	0.00260	953.7	113.7	979.1	34.4	998.4	14.3	−1.9
L262-1@02	81.14	207.57	0.39	0.06816	0.00271	1.25161	0.05174	0.13265	0.00188	873.1	82.6	824.1	23.3	803.0	10.7	2.6
L262-1@03	143.62	237.41	0.60	0.14283	0.00407	8.34913	0.25177	0.42241	0.00534	2262.0	48.6	2269.7	27.4	2271.4	24.2	−0.4
L262-1@04	149.01	285.92	0.52	0.05188	0.00245	0.27957	0.01312	0.03929	0.00052	279.7	107.4	250.3	10.4	248.5	3.2	0.8
L262-1@05	274.80	318.43	0.86	0.07846	0.00217	2.14510	0.06452	0.19794	0.00281	1158.3	55.6	1163.5	20.8	1164.3	15.1	−0.5
L262-1@06	61.81	147.87	0.42	0.16251	0.00445	10.56136	0.31695	0.46871	0.00570	2483.3	46.3	2485.3	27.8	2477.9	25.0	0.2
L262-1@07	36.19	60.67	0.60	0.19076	0.00535	13.74413	0.39843	0.52363	0.00751	2750.0	46.3	2732.2	27.4	2714.6	31.8	1.3
L262-1@08	62.61	61.25	1.02	0.11033	0.00373	4.89421	0.16788	0.32230	0.00419	1805.6	61.3	1801.3	28.9	1801.0	20.4	0.3
L262-1@09	61.28	76.90	0.80	0.24745	0.00600	21.25862	0.55763	0.61973	0.00723	3168.8	38.6	3150.5	25.4	3108.8	28.8	1.9
L262-1@10	138.34	266.51	0.52	0.05447	0.00219	0.53424	0.02262	0.07135	0.00097	390.8	90.7	434.6	15.0	444.3	5.9	−2.2
L262-1@11	139.77	73.26	1.91	0.17761	0.00506	11.69703	0.35340	0.47574	0.00583	2630.6	47.5	2580.5	28.3	2508.7	25.5	4.9
L262-1@12	207.20	309.59	0.67	0.09805	0.00337	3.48921	0.12620	0.25861	0.00439	1587.4	64.2	1524.8	28.6	1482.7	22.5	7.1
L262-1@13	323.51	1637.43	0.20	0.05633	0.00181	0.31194	0.01070	0.04290	0.00049	464.9	102.8	275.7	8.3	270.8	3.0	1.8
L262-1@14	98.89	443.18	0.22	0.11659	0.00311	5.19566	0.14573	0.32264	0.00359	1905.6	47.1	1851.9	23.9	1802.6	17.5	5.7
L262-1@15	170.60	270.37	0.63	0.05338	0.00244	0.49638	0.02129	0.06834	0.00095	346.4	108.3	409.3	14.4	426.2	5.7	−4.0
L262-1@16	25.72	70.94	0.36	0.18718	0.00628	12.72828	0.44399	0.49427	0.00684	2717.6	55.2	2659.8	32.9	2589.1	29.5	5.0
L262-1@17	**153.41**	**247.44**	**0.62**	**0.09507**	**0.00664**	**0.85164**	**0.06730**	**0.06399**	**0.00077**	**1529.3**	**131.8**	**625.5**	**36.9**	**399.9**	**4.7**	**56.4**
L262-1@18	133.28	306.62	0.43	0.07435	0.00212	1.82177	0.05482	0.17739	0.00206	1050.9	57.4	1053.3	19.7	1052.7	11.3	−0.2
L262-1@19	97.43	208.36	0.47	0.06285	0.00207	0.79768	0.02824	0.09225	0.00169	701.9	70.4	595.5	16.0	568.8	9.9	4.7
L262-1@20	610.08	1532.25	0.40	0.04872	0.00219	0.08671	0.00409	0.01289	0.00020	200.1	100.9	84.4	3.8	82.6	1.3	2.2
L262-1@21	37.84	169.73	0.22	0.07681	0.00254	2.00140	0.06843	0.18767	0.00246	1116.7	65.3	1116.0	23.2	1108.7	13.3	0.7
L262-1@22	249.73	249.38	1.00	0.06499	0.00215	1.16501	0.04086	0.12880	0.00173	773.8	70.4	784.3	19.2	781.0	9.9	0.4
L262-1@23	89.54	71.00	1.26	0.20163	0.00600	15.44488	0.46967	0.55154	0.00725	2839.2	48.8	2843.1	29.0	2831.6	30.1	0.3
L262-1@24	251.97	509.46	0.49	0.07083	0.00232	1.49490	0.04896	0.15205	0.00203	953.7	67.4	928.3	19.9	912.5	11.3	1.7
L262-1@25	95.47	153.87	0.62	0.05114	0.00381	0.26752	0.02036	0.03782	0.00079	255.6	172.2	240.7	16.3	239.3	4.9	0.6
L262-1@26	115.16	406.17	0.28	0.04905	0.00241	0.26200	0.01264	0.03849	0.00062	150.1	114.8	236.3	10.2	243.5	3.8	−3.0
L262-1@27	130.85	580.44	0.23	0.05442	0.00213	0.52119	0.02056	0.06860	0.00090	387.1	87.0	425.9	13.7	427.7	5.4	−0.4
L262-1@28	149.08	367.42	0.41	0.13490	0.00389	7.76678	0.23907	0.41095	0.00601	2162.7	45.4	2204.4	27.7	2219.2	27.4	−2.6
L262-1@29	138.39	309.65	0.45	0.16785	0.00478	10.68272	0.35160	0.45614	0.00752	2536.1	47.5	2495.9	30.6	2422.5	33.3	4.7
L262-1@30	42.64	293.77	0.15	0.12577	0.00380	6.16664	0.19336	0.34910	0.00428	2039.8	52.6	1999.7	27.4	1930.3	20.5	5.7
L262-1@31	140.37	173.68	0.81	0.11337	0.00353	5.23070	0.16610	0.32886	0.00432	1854.0	55.7	1857.6	27.1	1832.8	20.9	1.2
L262-1@32	194.10	305.37	0.64	0.05164	0.00250	0.31767	0.01551	0.04412	0.00069	333.4	111.1	280.1	12.0	278.3	4.3	0.6
L262-1@33	77.50	103.14	0.75	0.06825	0.00319	1.32426	0.06217	0.13909	0.00202	875.9	97.1	856.4	27.2	839.5	11.4	2.0
L262-1@34	51.18	55.33	0.93	0.11614	0.00441	5.39158	0.21085	0.33160	0.00553	1898.2	68.4	1883.5	33.5	1846.2	26.8	2.8
L262-1@35	**87.97**	**169.07**	**0.52**	**0.07496**	**0.00301**	**1.79866**	**0.07393**	**0.16934**	**0.00252**	**1133.3**	**80.7**	**1045.0**	**26.8**	**1008.4**	**13.9**	**12.4**
L262-1@36	64.37	143.85	0.45	0.05464	0.00324	0.53142	0.03153	0.06916	0.00105	398.2	133.3	432.8	20.9	431.1	6.3	0.4
L262-1@37	124.08	549.26	0.23	0.05103	0.00230	0.27793	0.01312	0.03836	0.00056	242.7	71.3	249.0	10.4	242.7	3.5	2.6
L262-1@38	113.66	229.12	0.50	0.05227	0.00291	0.27955	0.01511	0.03873	0.00063	298.2	127.8	250.3	12.0	244.9	3.9	2.2
L262-1@39	185.67	411.02	0.45	0.05381	0.00249	0.51313	0.02402	0.06685	0.00085	361.2	105.5	420.6	16.1	417.2	5.1	0.8
L262-1@40	370.74	429.25	0.86	0.04780	0.00272	0.16929	0.01008	0.02493	0.00040	100.1	120.4	158.8	8.8	158.7	2.5	0.0
L262-1@41	73.83	104.19	0.71	0.19301	0.00541	14.01132	0.39663	0.51819	0.00657	2768.2	46.0	2750.5	26.8	2691.5	27.9	2.8
L262-1@42	252.22	434.32	0.58	0.05562	0.00208	0.54652	0.02160	0.06953	0.00104	438.9	83.3	442.7	14.2	433.3	6.3	2.2
L262-1@43	108.81	758.78	0.14	0.05250	0.00178	0.27953	0.01001	0.04036	0.00081	305.6	77.8	250.3	7.9	255.1	5.0	−1.9
L262-1@44	551.06	729.62	0.76	0.07755	0.00219	1.90016	0.05430	0.17449	0.00188	1144.5	55.6	1081.1	19.0	1046.8	10.3	9.3
L262-1@45	103.76	564.87	0.18	0.05249	0.00239	0.29977	0.01359	0.04077	0.00053	305.6	105.5	266.2	10.6	257.6	3.3	3.3
L262-1@46	210.63	218.91	0.96	0.16390	0.00528	9.90179	0.31916	0.43240	0.00593	2496.0	53.6	2425.7	29.7	2316.5	26.7	7.7
L262-1@47	221.80	355.43	0.62	0.05623	0.00221	0.55816	0.02158	0.07152	0.00091	461.2	87.0	450.3	14.1	445.3	5.5	1.1
L262-1@48	79.09	106.09	0.75	0.09456	0.00354	3.12385	0.11793	0.23820	0.00333	1520.4	70.4	1438.6	29.0	1387.3	17.4	9.6
L262-1@49	159.09	198.69	0.80	0.05570	0.00260	0.53496	0.02540	0.06941	0.00101	438.9	105.5	435.1	16.8	432.6	6.1	0.6
L262-1@50	82.94	67.91	1.22	0.11565	0.00424	5.17008	0.18663	0.32415	0.00483	1900.0	60.7	1847.7	30.7	1810.0	23.5	5.0
L262-1@51	97.35	699.30	0.14	0.05555	0.00199	0.51724	0.01876	0.06723	0.00088	435.2	84.3	423.3	12.6	419.4	5.3	0.9
L262-1@52	225.53	309.13	0.73	0.05344	0.00213	0.49363	0.01993	0.06680	0.00097	346.4	90.7	407.4	13.5	416.9	5.9	−2.3
L262-1@53	516.91	632.38	0.82	0.05623	0.00191	0.62255	0.02152	0.07984	0.00101	461.2	108.3	491.4	13.5	495.2	6.1	−0.8

Table 1 (continued)

Grain no.	Element (ppm)		Th/U	Ratios						Age (Ma)						Discordant text
	Th	U		$^{207}Pb/^{206}Pb$	1σ	$^{207}Pb/^{235}U$	1σ	$^{206}Pb/^{238}U$	1σ	$^{207}Pb/^{206}Pb$	1σ	$^{207}Pb/^{235}U$	1σ	$^{206}Pb/^{238}U$	1σ	
L262-1@54	87.30	436.02	0.20	0.06345	0.00223	1.13504	0.04173	0.12891	0.00189	724.1	70.2	770.2	19.8	781.6	10.8	−1.5
L262-1@55	453.84	405.87	1.12	0.04985	0.00231	0.36520	0.01723	0.05270	0.00079	187.1	112.0	316.1	12.8	331.1	4.8	−4.5
L262-1@56	275.06	370.47	0.74	0.05229	0.00244	0.49184	0.02356	0.06744	0.00101	298.2	139.8	406.2	16.0	420.7	6.1	−3.5
L262-1@57	44.62	211.17	0.21	0.10786	0.00358	4.92402	0.16659	0.32762	0.00427	1764.8	65.7	1806.4	28.6	1826.9	20.7	−3.4
L262-1@58	188.47	309.27	0.61	0.05389	0.00223	0.51768	0.02236	0.06893	0.00098	364.9	62.0	423.6	15.0	429.7	5.9	−1.4
L262-1@59	63.45	377.66	0.17	0.05152	0.00202	0.48550	0.01932	0.06769	0.00086	264.9	90.7	401.8	13.2	422.2	5.2	−4.8
L262-1@60	323.28	245.02	1.32	0.06252	0.00248	0.97415	0.03819	0.11214	0.00158	700.0	85.2	690.6	19.6	685.2	9.2	0.8
L262-1@61	72.03	211.95	0.34	0.04917	0.00302	0.25586	0.01544	0.03738	0.00058	166.8	144.4	231.3	12.5	236.6	3.6	−2.2
L262-1@62	62.65	149.16	0.42	0.11575	0.00385	5.23292	0.17409	0.32442	0.00419	1891.7	59.4	1858.0	28.4	1811.3	20.4	4.4
L262-1@63	64.75	199.87	0.32	0.11363	0.00391	5.14381	0.18304	0.32435	0.00458	1858.3	62.8	1843.4	30.3	1811.0	22.3	2.6
L262-1@64	71.84	121.00	0.59	0.16344	0.00594	10.47549	0.38661	0.45965	0.00639	2491.7	61.1	2477.8	34.2	2438.0	28.2	2.2
L262-1@65	56.54	123.64	0.46	0.16114	0.00649	9.50080	0.38970	0.42285	0.00631	2477.8	101.1	2387.6	37.7	2273.4	28.6	9.0
L262-1@66	199.28	294.09	0.68	0.05086	0.00317	0.27460	0.01688	0.03902	0.00065	235.3	144.4	246.4	13.4	246.8	4.1	−0.2
L262-1@67	55.14	338.67	0.16	0.05389	0.00275	0.49822	0.02536	0.06670	0.00104	364.9	110.2	410.5	17.2	416.2	6.3	−1.4
L262-1@68	20.75	377.02	0.06	0.18482	0.00635	12.88931	0.46577	0.50063	0.00731	2698.2	57.6	2671.6	34.1	2616.5	31.4	3.1
L262-1@69	157.74	211.00	0.75	0.06755	0.00309	1.08102	0.04712	0.11960	0.00207	853.7	89.8	744.1	23.0	728.2	11.9	2.2
L262-1@70	**160.92**	**512.18**	**0.31**	**0.15912**	**0.00558**	**8.22590**	**0.30316**	**0.37088**	**0.00467**	**2446.6**	**59.3**	**2256.2**	**33.4**	**2033.5**	**22.0**	**20.3**
L262-1@71	151.88	245.06	0.62	0.05456	0.00249	0.53275	0.02513	0.07048	0.00103	394.5	103.7	433.6	16.6	439.1	6.2	−1.2
L262-1@72	418.56	798.52	0.52	0.05319	0.00213	0.27223	0.01090	0.03679	0.00045	344.5	95.4	244.5	8.7	232.9	2.8	5.0
L262-1@73	51.27	81.12	0.63	0.11814	0.00416	5.40662	0.18601	0.33051	0.00477	1928.1	63.0	1885.9	29.5	1840.9	23.1	4.7
L262-1@74	264.22	394.16	0.67	0.08500	0.00274	2.48881	0.08156	0.20934	0.00246	1316.7	62.7	1268.8	23.7	1225.3	13.1	7.5
L262-1@75	211.71	490.54	0.43	0.12698	0.00409	6.06233	0.19855	0.34127	0.00471	2057.4	61.9	1984.8	28.6	1892.8	22.7	8.7
L262-1@76	104.43	191.64	0.54	0.06681	0.00292	1.11571	0.04819	0.12052	0.00188	831.5	90.7	760.9	23.1	733.5	10.8	3.7
L262-1@77	15.44	22.25	0.69	0.11595	0.00605	4.93877	0.26269	0.31159	0.00609	1894.8	94.4	1808.9	44.9	1748.5	29.9	8.4
L262-1@78	155.00	318.99	0.49	0.05598	0.00232	0.53430	0.02202	0.06917	0.00098	450.0	88.0	434.7	14.6	431.2	5.9	0.8
L262-1@79	64.19	209.63	0.31	0.05352	0.00290	0.43164	0.02477	0.05833	0.00093	350.1	122.2	364.3	17.6	365.5	5.7	−0.3
L262-1@80	347.12	864.54	0.40	0.20367	0.00656	14.38252	0.53195	0.51228	0.00878	2857.4	52.5	2775.3	35.1	2666.4	37.4	7.2
L262-1@81	135.41	194.42	0.70	0.06472	0.00271	1.09314	0.04981	0.12309	0.00176	764.8	87.0	750.0	24.2	748.4	10.1	0.2
L262-1@82	70.51	43.70	1.61	0.09994	0.00484	3.81515	0.18623	0.28202	0.00466	1633.3	89.3	1595.9	39.3	1601.5	23.4	2.0
L262-1@83	50.71	112.97	0.45	0.06305	0.00292	1.05949	0.05067	0.12345	0.00184	709.3	98.1	733.6	25.0	750.4	10.5	−2.2
L262-1@84	75.55	208.52	0.36	0.10672	0.00335	4.65439	0.15600	0.31849	0.00408	1744.1	62.0	1759.1	28.0	1782.4	19.9	−2.1
L262-1@85	175.29	251.14	0.70	0.06182	0.00269	1.06574	0.04757	0.12615	0.00182	733.3	97.2	736.6	23.4	765.9	10.4	−3.8
L262-1@86	296.78	295.92	1.00	0.05278	0.00277	0.49832	0.02781	0.06857	0.00110	320.4	120.4	410.6	18.8	427.6	6.6	−4.0
L262-1@87	298.94	575.60	0.52	0.07230	0.00242	1.71416	0.06102	0.17063	0.00207	994.4	68.5	1013.8	22.8	1015.6	11.4	−2.1
L262-1@88	83.21	202.88	0.41	0.13920	0.00455	7.83337	0.27053	0.40332	0.00501	2217.6	56.0	2212.0	31.1	2184.3	23.0	1.5
L262-1@89	245.65	426.95	0.58	0.05093	0.00276	0.30502	0.01681	0.04321	0.00067	239.0	128.7	270.3	13.1	272.7	4.1	−0.9
L262-1@90	155.54	205.67	0.76	0.05041	0.00329	0.26399	0.01825	0.03691	0.00062	213.0	154.6	237.9	14.7	233.7	3.8	1.8
Sample: L262-2																
L262-2@01	401.92	378.28	1.06	0.04977	0.00373	0.10626	0.00781	0.01556	0.00029	183.4	166.6	102.5	7.2	99.5	1.8	3.0
L262-2@02	211.27	282.87	0.75	0.04920	0.00370	0.10493	0.00746	0.01536	0.00030	166.8	157.4	101.3	6.9	98.3	1.9	3.1
L262-2@03	676.58	529.37	1.28	0.04782	0.00309	0.09969	0.00653	0.01504	0.00026	100.1	135.2	96.5	6.0	96.2	1.6	0.3
L262-2@04	109.49	142.82	0.77	0.05612	0.00603	0.09926	0.00763	0.01471	0.00044	457.5	240.7	96.1	7.0	94.1	2.8	2.1
L262-2@05	197.86	497.47	0.40	0.05186	0.00178	0.27925	0.01040	0.03830	0.00053	279.7	84.2	250.1	8.3	242.3	3.3	3.2
L262-2@06	73.97	129.35	0.57	0.05329	0.00371	0.25636	0.01637	0.03698	0.00082	342.7	162.0	231.7	13.2	234.1	5.1	−1.0
L262-2@07	134.03	154.10	0.87	0.05097	0.00364	0.25691	0.01727	0.03722	0.00073	239.0	164.8	232.2	14.0	235.6	4.5	−1.5
L262-2@08	213.81	357.70	0.60	0.04797	0.00340	0.09877	0.00695	0.01498	0.00025	98.2	159.2	95.6	6.4	95.8	1.6	−0.2
L262-2@09	107.26	135.47	0.79	0.04882	0.00425	0.10187	0.00878	0.01518	0.00044	139.0	192.6	98.5	8.1	97.1	2.8	1.4
L262-2@10	176.88	326.81	0.54	0.04854	0.00248	0.23990	0.01269	0.03565	0.00056	124.2	−78.7	218.3	10.4	225.8	3.5	−3.3
L262-2@11	82.39	144.43	0.57	0.05135	0.00364	0.25860	0.01825	0.03714	0.00079	257.5	164.8	233.5	14.7	235.1	4.9	−0.7
L262-2@12	32.68	81.62	0.40	0.05266	0.00430	0.26347	0.02046	0.03728	0.00091	322.3	191.6	237.5	16.4	236.0	5.6	0.6
L262-2@13	201.15	344.45	0.58	0.04914	0.00337	0.10684	0.00728	0.01584	0.00030	153.8	155.5	103.1	6.7	101.3	1.9	1.7
L262-2@14	59.00	65.62	0.90	0.05093	0.00411	0.27239	0.02491	0.03852	0.00091	239.0	187.0	244.6	19.9	243.6	5.6	0.4
L262-2@15	547.48	398.01	1.38	0.04747	0.00350	0.10278	0.00799	0.01551	0.00031	72.3	166.6	99.3	7.4	99.2	2.0	0.1
L262-2@16	275.53	549.43	0.50	0.04890	0.00241	0.26006	0.01282	0.03828	0.00063	142.7	110.2	234.7	10.3	242.2	3.9	−3.1
L262-2@17	248.19	565.02	0.44	0.04862	0.00245	0.26394	0.01325	0.03897	0.00057	127.9	118.5	237.8	10.6	246.4	3.5	−3.5
L262-2@18	32.07	98.28	0.33	0.05229	0.00448	0.27185	0.02312	0.03831	0.00090	298.2	191.6	244.2	18.5	242.3	5.6	0.8

L262-2@19	130.06	241.82	0.54	0.05069	0.00321	0.25877	0.01633	0.03700	0.00065	233.4	148.1	233.7	13.2	234.2	4.1	−0.2
L262-2@20	95.55	87.90	1.09	0.05203	0.00407	0.27196	0.02198	0.03834	0.00078	287.1	179.6	244.3	17.6	242.5	4.8	0.7
L262-2@21	503.65	577.73	0.87	0.04800	0.00262	0.10179	0.00552	0.01516	0.00025	98.2	135.2	98.4	5.1	97.0	1.6	1.5
L262-2@22	122.65	156.21	0.79	0.04971	0.00571	0.10173	0.00975	0.01554	0.00039	189.0	238.9	98.4	9.0	99.4	2.5	−1.0
L262-2@23	152.72	142.79	1.07	0.04982	0.00545	0.10086	0.01044	0.01502	0.00042	187.1	246.3	97.6	9.6	96.1	2.7	1.6
L262-2@24	533.03	768.37	0.69	0.05168	0.00189	0.28646	0.01143	0.03931	0.00055	272.3	83.3	255.8	9.0	248.6	3.4	2.9
L262-2@25	469.86	755.38	0.62	0.04802	0.00287	0.10475	0.00638	0.01563	0.00023	101.9	133.3	101.2	5.9	100.0	1.4	1.2
L262-2@26	241.78	218.13	1.11	0.04963	0.00373	0.10332	0.00741	0.01564	0.00036	176.0	166.6	99.8	6.8	100.0	2.3	−0.2
L262-2@27	272.38	356.72	0.76	0.04982	0.00343	0.10191	0.00652	0.01525	0.00027	187.1	161.1	98.5	6.0	97.6	1.7	1.0
L262-2@28	174.39	583.24	0.30	0.05205	0.00213	0.28813	0.01193	0.03952	0.00052	287.1	99.1	257.1	9.4	249.8	3.3	2.9
L262-2@29	83.20	98.77	0.84	0.05134	0.00440	0.26542	0.02407	0.03729	0.00087	257.5	193.5	239.0	19.3	236.0	5.4	1.3
L262-2@30	140.94	218.31	0.65	0.05124	0.00301	0.26736	0.01650	0.03744	0.00068	250.1	139.8	240.6	13.2	236.9	4.2	1.5
L262-2@31	328.23	568.68	0.58	0.05129	0.00224	0.27392	0.01179	0.03830	0.00051	253.8	100.0	245.8	9.4	242.3	3.1	1.5
L262-2@32	163.61	205.46	0.80	0.04998	0.00466	0.10290	0.00978	0.01529	0.00036	194.5	203.7	99.4	9.0	97.8	2.3	1.7
L262-2@33	258.31	404.35	0.64	0.04918	0.00375	0.10232	0.00732	0.01541	0.00028	166.8	157.4	98.9	6.7	98.6	1.8	0.3
L262-2@34	150.14	231.54	0.65	0.04885	0.00439	0.10393	0.00917	0.01559	0.00034	139.0	200.0	100.4	8.4	99.7	2.2	0.7
L262-2@35	178.94	184.51	0.97	0.05010	0.00571	0.10229	0.00946	0.01540	0.00036	198.2	257.4	98.9	8.7	98.5	2.3	0.4
L262-2@36	135.65	232.54	0.58	0.05227	0.00314	0.26512	0.01500	0.03713	0.00069	298.2	137.0	238.8	12.0	235.0	4.3	1.6
L262-2@37	320.82	455.32	0.70	0.05349	0.00238	0.39126	0.01962	0.05260	0.00137	350.1	100.0	335.3	14.3	330.4	8.4	1.5
L262-2@38	352.78	625.64	0.56	0.05172	0.00227	0.26687	0.01258	0.03695	0.00051	272.3	101.8	240.2	10.1	233.9	3.2	2.7
L262-2@39	123.36	350.21	0.35	0.05191	0.00255	0.27954	0.01422	0.03900	0.00056	279.7	112.9	250.3	11.3	246.6	3.5	1.5
L262-2@40	213.59	667.84	0.32	0.05113	0.00209	0.27864	0.01178	0.03934	0.00049	255.6	94.4	249.6	9.4	248.8	3.0	0.3
L262-2@41	255.34	276.98	0.92	0.05028	0.00410	0.10492	0.00761	0.01576	0.00029	209.3	190.7	101.3	7.0	100.8	1.9	0.5
L262-2@42	109.76	139.97	0.78	0.05259	0.00402	0.26632	0.01912	0.03749	0.00069	309.3	174.1	239.7	15.3	237.3	4.3	1.0
L262-2@43	251.59	342.02	0.74	0.04793	0.00316	0.10634	0.00712	0.01594	0.00029	94.5	161.1	102.6	6.5	102.0	1.8	0.6
L262-2@44	69.31	136.90	0.51	0.05155	0.00359	0.26136	0.01771	0.03700	0.00076	264.9	159.2	235.8	14.3	234.2	4.7	0.7
L262-2@45	210.46	271.07	0.78	0.04858	0.00367	0.10656	0.00784	0.01578	0.00032	127.9	170.3	102.8	7.2	101.0	2.0	1.8
L262-2@46	192.25	163.48	1.18	0.05129	0.00591	0.10435	0.01090	0.01534	0.00050	253.8	244.4	100.8	10.0	98.2	3.2	2.7
L262-2@47	144.49	229.40	0.63	0.05118	0.00294	0.27484	0.01595	0.03828	0.00070	255.6	133.3	246.6	12.7	242.2	4.3	1.8
L262-2@48	427.99	1580.12	0.27	0.05225	0.00177	0.28089	0.01024	0.03851	0.00059	294.5	77.8	251.4	8.1	243.6	3.7	3.2
L262-2@49	23.17	41.02	0.56	0.05784	0.00694	0.30671	0.02982	0.04304	0.00112	524.1	266.6	271.6	23.2	271.7	6.9	0.0
L262-2@50	116.36	171.54	0.68	0.04873	0.00362	0.10192	0.00712	0.01535	0.00036	200.1	101.8	98.5	6.6	98.2	2.3	0.4
L262-2@51	56.09	108.60	0.52	0.05149	0.00445	0.10150	0.00571	0.01524	0.00041	261.2	200.0	98.2	5.3	97.5	2.6	0.7
L262-2@52	430.91	505.33	0.85	0.04910	0.00325	0.09821	0.00610	0.01463	0.00024	153.8	148.1	95.1	5.6	93.6	1.5	1.6
L262-2@53	132.18	196.96	0.67	0.05166	0.00326	0.25318	0.01565	0.03556	0.00063	333.4	144.4	229.2	12.7	225.2	3.9	1.7
L262-2@54	43.05	86.94	0.50	0.05194	0.00427	0.26502	0.02115	0.03745	0.00081	283.4	188.9	238.7	17.0	237.0	5.0	0.7
L262-2@55	208.52	304.07	0.69	0.04820	0.00403	0.10305	0.00834	0.01556	0.00028	109.4	185.2	99.6	7.7	99.6	1.8	0.0
L262-2@56	92.87	284.76	0.33	0.05062	0.00263	0.28329	0.01479	0.03986	0.00063	233.4	120.4	253.3	11.7	252.0	3.9	0.5
L262-2@57	252.79	568.33	0.44	0.05131	0.00240	0.27603	0.01333	0.03845	0.00052	253.8	112.0	247.5	10.6	243.2	3.3	1.8
L262-2@58	500.43	498.95	1.00	0.04973	0.00375	0.10014	0.00728	0.01491	0.00026	189.0	161.1	96.9	6.7	95.4	1.6	1.6
L262-2@59	429.51	536.30	0.80	0.05126	0.00201	0.28183	0.01184	0.03922	0.00055	253.8	86.1	252.1	9.4	248.0	3.4	1.6
L262-2@60	257.24	220.58	1.17	0.04805	0.00395	0.09988	0.00868	0.01478	0.00031	101.9	185.2	96.7	8.0	94.6	1.9	2.2
L262-2@61	261.50	338.32	0.77	0.04838	0.00353	0.10349	0.00772	0.01551	0.00031	116.8	162.9	100.0	7.1	99.2	2.0	0.8
L262-2@62	174.94	288.04	0.61	0.04767	0.00317	0.10467	0.00765	0.01567	0.00031	83.4	151.8	101.1	7.0	100.2	1.9	0.8
L262-2@63	175.80	244.33	0.72	0.05092	0.00459	0.10348	0.00868	0.01557	0.00035	239.0	207.4	100.0	8.0	99.6	2.2	0.4
L262-2@64	194.13	320.41	0.61	0.09108	0.00257	3.13106	0.08978	0.24725	0.00283	1450.0	53.7	1440.4	22.1	1424.3	14.6	1.8
L262-2@65	223.67	406.11	0.55	0.05057	0.00242	0.26628	0.01293	0.03746	0.00054	220.4	111.1	239.7	10.4	237.1	3.4	1.1
L262-2@66	211.17	248.71	0.85	0.05089	0.00388	0.10284	0.00761	0.01550	0.00035	235.3	205.5	99.4	7.0	99.1	2.2	0.3
L262-2@67	311.76	277.24	1.12	0.05137	0.00425	0.10499	0.00865	0.01557	0.00035	257.5	190.7	101.4	7.9	99.6	2.2	1.8
L262-2@68	77.39	131.74	0.59	0.05156	0.00353	0.25832	0.01851	0.03701	0.00074	264.9	157.4	233.3	14.9	234.3	4.6	−0.4
L262-2@69	71.18	148.99	0.48	0.05172	0.00324	0.27700	0.01714	0.03870	0.00071	272.3	142.6	248.3	13.6	244.8	4.4	1.4
L262-2@70	553.53	977.44	0.57	0.05047	0.00161	0.26331	0.00873	0.03752	0.00046	216.7	78.7	237.3	7.0	237.4	2.8	0.0
L262-2@71	284.85	375.37	0.76	0.04814	0.00332	0.10504	0.00721	0.01602	0.00029	105.6	155.5	101.4	6.6	102.4	1.8	−1.0
L262-2@72	221.22	557.40	0.40	0.04942	0.00187	0.27464	0.01050	0.04023	0.00057	168.6	88.9	246.4	8.4	254.2	3.6	−3.1
L262-2@73	135.62	153.09	0.89	0.05078	0.00304	0.27246	0.01821	0.03778	0.00072	231.6	138.9	244.7	14.5	239.1	4.4	2.3
L262-2@74	137.97	389.44	0.35	0.05133	0.00243	0.27333	0.01276	0.03872	0.00052	257.5	109.2	245.3	10.2	244.9	3.2	0.2
L262-2@75	163.07	377.20	0.43	0.05194	0.00235	0.27854	0.01311	0.03862	0.00056	283.4	103.7	249.5	10.4	244.3	3.5	2.1
L262-2@76	638.25	534.61	1.19	0.05051	0.00312	0.10296	0.00646	0.01464	0.00024	220.4	137.9	99.5	5.9	93.7	1.5	6.2
L262-2@77	520.95	446.15	1.17	0.04888	0.00234	0.10521	0.00478	0.01574	0.00026	142.7	108.3	101.6	4.4	100.7	1.7	0.9

Table 1 (continued)

Grain no.	Element (ppm)		Th/U	Ratios						Age (Ma)						Discordant text
	Th	U		^{207}Pb/^{206}Pb	1σ	^{207}Pb/^{235}U	1σ	^{206}Pb/^{238}U	1σ	^{207}Pb/^{206}Pb	1σ	^{207}Pb/^{235}U	1σ	^{206}Pb/^{238}U	1σ	
L262-2@78	74.40	253.10	0.29	0.05153	0.00279	0.28613	0.01501	0.04038	0.00064	264.9	91.7	255.5	11.9	255.2	4.0	0.1
L262-2@79	161.47	237.52	0.68	0.05087	0.00402	0.10443	0.00776	0.01546	0.00033	235.3	183.3	100.9	7.1	98.9	2.1	2.0
L262-2@80	175.02	282.99	0.62	0.05104	0.00266	0.26182	0.01383	0.03701	0.00058	242.7	125.0	236.1	11.1	234.3	3.6	0.8
L262-2@81	169.39	298.36	0.57	0.04866	0.00380	0.10330	0.00756	0.01560	0.00024	131.6	174.0	99.8	7.0	99.8	1.6	0.1
L262-2@82	136.24	196.97	0.69	0.05087	0.00301	0.26611	0.01707	0.03772	0.00061	235.3	132.4	239.6	13.7	238.7	3.8	0.4
L262-2@83	248.68	555.70	0.45	0.05125	0.00195	0.26096	0.01075	0.03634	0.00045	253.8	91.7	235.4	8.7	230.1	2.8	2.3
L262-2@84	138.94	209.94	0.66	0.04959	0.00386	0.10417	0.00818	0.01560	0.00034	176.0	174.0	100.6	7.5	99.8	2.2	0.8
L262-2@85	48.67	73.46	0.66	0.09153	0.00294	3.11031	0.10146	0.24756	0.00371	1457.7	61.1	1435.2	25.1	1425.9	19.2	2.2

(Table 2 and Fig. 7A). The Hf isotopic model ages (T_{DM2}) for these zircons range from 3.22 to 1.16 Ga (Table 2 and Fig. 8A).

Twenty-five spots were made on 25 zircon grains from sample L262-2. The results show a relatively narrow range of initial ^{176}Hf/^{177}Hf ratios from 0.2818 to 0.2826, with $\varepsilon_{Hf}(t)$ values of −11.6 to 0.6 (Table 2 and Fig. 7B). The Hf isotopic model ages (T_{DM2}) for these zircons range from 2.07 to 1.10 Ga, with a concentration in 1.5–1.1 Ga (Table 2 and Fig. 8B).

5. Discussion

5.1. Source characteristics of surrounding tectonic units

The hinterland of the southern Yangtze Block, the Truong Son Belt (Indochina Block) and the Hainan Uplift (Cathaysia Block) (Fig. 1A) all constitute potential sedimentary sources for the Y-SH Basin during the Late Miocene (Xie, 2009; Wang et al., 2014). Understanding the provenance characteristics of these tectonic units is an important factor in determining the provenance of the studied samples.

The basement rocks of the southern Yangtze Block are of Proterozoic and Archean age (2100–1700 Ma and 2800–2300 Ma, respectively) (Metcalfe, 2006; Zheng et al., 2006). The block is characterized by Neoproterozoic magmatic activity (1000–700 Ma) (Chen and Jahn, 1998; Huang et al., 2009), probably in response to the breakup of Rodinia (Li et al., 2003; Ling et al., 2003). U–Pb ages of Late Paleozoic igneous rocks in the Youjiang Basin and Song Chay Massif range from 480 to 400 Ma (Roger et al., 2000; Carter et al., 2001; Yan et al., 2006; Yang et al., 2012a,b). Mesozoic igneous rocks associated with the Emeishan mantle plume, or collision between several micro-continents and the Yangtze Craton are found to yield U–Pb ages between 280 and 220 Ma (Hoa et al., 2008; Zhong et al., 2009; Zhong and Xu, 2009; Roger et al., 2012; Chen et al., 2014). The distributions of igneous rocks in this area are shown in Figure 9 (area A).

The Truong Son Belt is characterized by Silurian and Permian–Triassic granites, which correspond to the Caledonian and Indosinian Orogenic Events, respectively (Fig. 9, area B). Rocks of early Permian–Triassic arc magmatism (280–270 Ma and 250–240 Ma) are widely distributed in this belt (Hoa et al., 2008; Liu et al., 2012). In addition, the Early Paleozoic granitoids within the Truong Son Belt are mainly located in the southwest of the orogenic belt, with ages of 460–430 Ma (Carter et al., 2001; Lan et al., 2003; Usuki et al., 2009).

The Permian to Triassic granitoids are well developed in the Hainan Uplift, on the southern margin of the Cathaysia Block (Fig. 9, area C). Representative igneous intrusions include the Jianfengling granite (249 Ma), Shilu granite (262 Ma), Panyangdong granite (234 Ma), Changtangling granite (264 Ma), Baolang granite (272 Ma), Tianzai granite (245 Ma) and Zhizhong granite (272 Ma) (Li et al., 2006; Xie et al., 2006a, 2006b; Wen, 2013; Wen et al., 2013). The Yanshanian granitoids are mainly distributed in the southern and western parts of Hainan Island, and their U–Pb ages are mainly in the range of 170–80 Ma (Wang et al., 1991, 2011, 2015; Jia et al., 2009).

5.2. Provenance analysis of detrital zircon

Sedimentary detritus in the study area was presumably transported by paleo-fluvial systems (e.g. Red River, Ma River, Changhua River) surrounding the basin and was subsequently reworked during transgressions (Xie, 2009). U–Pb ages of detrital zircon have been widely used in detecting the provenance of geologic terranes and sedimentary sequences (Yang et al., 2012a,b). The U–Pb Concordia plots (Fig. 6) display striking age differences between the

Table 2
Hf isotopic data of the detrital zircons from the Y-SH Basin.

Grain no.	Age (Ma)	$^{176}Yb/^{177}Hf$	2σ	$^{176}Lu/^{177}Hf$	2σ	$^{176}Hf/^{177}Hf$	2σ	$^{176}Hf/^{177}Hf_i$	$\varepsilon_{Hf}(t)$	2σ	T_{DM1} (Ma)	T_{DM2} (Ma)	TDMC (Ma)	$f_{Lu/Hf}$
Sample: L262-1														
L262-1@01	998	0.027218	0.000169	0.000633	0.000005	0.282149	0.000014	0.282137	−0.38	0.48	1541	1692	1889	−0.98
L262-1@05	1158	0.054092	0.000277	0.001310	0.000003	0.282114	0.000015	0.282085	1.35	0.51	1618	1738	1903	−0.96
L262-1@08	1806	0.011021	0.000041	0.000243	0.000001	0.281524	0.000013	0.281524	−3.93	0.46	2361	2534	2741	−0.99
L262-1@13	271	0.046288	0.000526	0.001222	0.000012	0.281821	0.000016	0.281815	−27.91	0.55	2022	2438	3042	−0.96
L262-1@15	426	0.051154	0.001081	0.001215	0.000020	0.282408	0.000015	0.282398	−3.85	0.52	1200	1390	1663	−0.96
L262-1@16	2718	0.011584	0.000096	0.000300	0.000002	0.281100	0.000013	0.281084	1.35	0.47	2944	3021	3107	−0.99
L262-1@25	239	0.031626	0.000485	0.000780	0.000013	0.282395	0.000017	0.282391	−8.22	0.59	1206	1451	1793	−0.98
L262-1@27	428	0.058979	0.003529	0.001620	0.000103	0.282288	0.000018	0.282275	−8.18	0.63	1384	1605	1938	−0.95
L262-1@29	2536	0.038613	0.000587	0.001042	0.000018	0.281190	0.000017	0.281140	−0.85	0.59	2877	2982	3109	−0.97
L262-1@31	1854	0.029698	0.000294	0.000716	0.000009	0.281361	0.000013	0.281336	−9.52	0.45	2623	2850	3132	−0.98
L262-1@36	431	0.025569	0.000316	0.000685	0.000008	0.282534	0.000016	0.282529	0.87	0.55	1008	1161	1368	−0.98
L262-1@37	243	0.060431	0.000373	0.001511	0.000005	0.282130	0.000015	0.282123	−17.63	0.52	1604	1915	2384	−0.95
L262-1@38	245	0.028909	0.000344	0.000690	0.000009	0.282373	0.000016	0.282370	−8.85	0.57	1233	1487	1837	−0.98
L262-1@39	417	0.065899	0.000447	0.001551	0.000003	0.282352	0.000014	0.282340	−6.12	0.50	1291	1495	1800	−0.95
L262-1@42	433	0.059256	0.000799	0.001503	0.000016	0.282158	0.000017	0.282146	−12.63	0.58	1564	1829	2222	−0.95
L262-1@43	255	0.096002	0.000923	0.002302	0.000015	0.282085	0.000015	0.282074	−19.09	0.53	1703	1997	2485	−0.93
L262-1@49	445	0.062570	0.000284	0.001490	0.000006	0.281838	0.000017	0.281826	−23.69	0.58	2012	2378	2919	−0.96
L262-1@47	433	0.095006	0.000721	0.002301	0.000031	0.282283	0.000017	0.282264	−8.46	0.59	1418	1623	1959	−0.93
L262-1@54	782	0.009136	0.000162	0.000240	0.000003	0.281618	0.000020	0.281615	−23.72	0.69	2245	2659	3184	−0.99
L262-1@56	421	0.052576	0.000700	0.001260	0.000025	0.282270	0.000019	0.282260	−8.88	0.66	1397	1634	1977	−0.96
L262-1@57	1765	0.027623	0.000326	0.000696	0.000007	0.281489	0.000013	0.281466	−6.93	0.47	2447	2649	2899	−0.98
L262-1@62	1892	0.049306	0.001212	0.001185	0.000031	0.281793	0.000016	0.281751	6.07	0.56	2059	2108	2169	−0.96
L262-1@64	2492	0.014829	0.000036	0.000428	0.000001	0.281283	0.000013	0.281263	2.48	0.45	2708	2779	2861	−0.99
L262-1@65	2478	0.018334	0.000512	0.000466	0.000013	0.281293	0.000019	0.281271	2.45	0.65	2698	2769	2853	−0.99
L262-1@68	2698	0.040510	0.000679	0.001086	0.000015	0.281030	0.000018	0.280974	−3.01	0.64	3099	3222	3371	−0.97
L262-1@81	748	0.016552	0.000208	0.000459	0.000004	0.282156	0.000015	0.282150	−5.51	0.51	1524	1739	2020	−0.99
L262-1@83	750	0.024878	0.000226	0.000647	0.000008	0.282050	0.000019	0.282041	−9.34	0.67	1678	1930	2262	−0.98
L262-1@87	994	0.039189	0.000202	0.000955	0.000006	0.281866	0.000017	0.281848	−10.71	0.59	1946	2199	2539	−0.97
L262-1@90	234	0.027936	0.000112	0.000668	0.000003	0.282411	0.000013	0.282408	−7.76	0.46	1180	1424	1760	−0.98
Sample: L262-2														
L262-2@02	98	0.028726	0.000164	0.000757	0.000003	0.282608	0.000015	0.282606	−3.70	0.51	907	1111	1398	−0.98
L262-2@03	96	0.082721	0.001231	0.001946	0.000024	0.282389	0.000019	0.282385	−11.57	0.65	1252	1497	1891	−0.94
L262-2@07	236	0.032894	0.001076	0.000789	0.000022	0.282474	0.000014	0.282471	−5.48	0.49	1095	1313	1618	−0.98
L262-2@13	101	0.028264	0.000354	0.000753	0.000013	0.282567	0.000015	0.282566	−5.07	0.53	963	1181	1486	−0.98
L262-2@16	242	0.027582	0.000066	0.000671	0.000002	0.282485	0.000013	0.282482	−4.95	0.45	1077	1292	1589	−0.98
L262-2@21	97	0.027838	0.000141	0.000731	0.000002	0.282605	0.000013	0.282604	−3.83	0.45	910	1116	1405	−0.98
L262-2@28	250	0.021144	0.000063	0.000512	0.000002	0.282482	0.000014	0.282480	−4.86	0.49	1076	1294	1589	−0.98
L262-2@29	236	0.038115	0.001139	0.000918	0.000022	0.282411	0.000014	0.282407	−7.72	0.52	1187	1424	1759	−0.97
L262-2@30	237	0.029459	0.000235	0.000707	0.000007	0.282404	0.000015	0.282401	−7.94	0.53	1191	1435	1774	−0.98
L262-2@43	102	0.043253	0.000425	0.001150	0.000008	0.282570	0.000015	0.282568	−4.98	0.52	970	1178	1482	−0.97
L262-2@47	242	0.038287	0.000232	0.000928	0.000008	0.282384	0.000013	0.282380	−8.55	0.45	1225	1470	1816	−0.97
L262-2@48	244	0.074742	0.000503	0.001838	0.000007	0.282447	0.000013	0.282439	−6.43	0.46	1164	1367	1684	−0.94
L262-2@52	94	0.053159	0.000536	0.001402	0.000012	0.282548	0.000014	0.282546	−5.96	0.49	1008	1219	1537	−0.96
L262-2@55	100	0.054393	0.001379	0.001326	0.000028	0.282570	0.000016	0.282567	−5.06	0.57	975	1180	1485	−0.96
L262-2@56	252	0.027395	0.000318	0.000679	0.000004	0.282340	0.000014	0.282337	−9.86	0.50	1278	1542	1906	−0.98
L262-2@63	100	0.029178	0.000481	0.000766	0.000009	0.282602	0.000014	0.282600	−3.89	0.50	916	1122	1411	−0.98
L262-2@64	1450	0.028629	0.000059	0.000710	0.000000	0.281866	0.000013	0.281847	−0.54	0.45	1933	2073	2250	−0.98
L262-2@71	102	0.040484	0.000203	0.001030	0.000007	0.282536	0.000016	0.282534	−6.18	0.54	1015	1237	1557	−0.97
L262-2@73	239	0.021785	0.000278	0.000512	0.000007	0.282490	0.000014	0.282488	−4.79	0.50	1064	1282	1577	−0.98
L262-2@77	101	0.046197	0.000462	0.001181	0.000007	0.282576	0.000015	0.282574	−4.80	0.52	962	1167	1469	−0.96
L262-2@78	255	0.038116	0.000502	0.000941	0.000007	0.282313	0.000014	0.282309	−10.78	0.49	1324	1590	1967	−0.97
L262-2@79	99	0.026163	0.000291	0.000678	0.000009	0.282617	0.000013	0.282615	−3.37	0.46	893	1095	1377	−0.98
L262-2@82	239	0.035249	0.000495	0.000851	0.000013	0.282386	0.000014	0.282382	−8.55	0.49	1220	1467	1814	−0.97
L262-2@83	230	0.025484	0.000249	0.000600	0.000005	0.282388	0.000013	0.282385	−8.63	0.46	1209	1464	1812	−0.98
L262-2@85	1458	0.021285	0.000412	0.000514	0.000008	0.281888	0.000013	0.281874	0.60	0.46	1894	2023	2183	−0.98

two samples, suggesting that they were derived from different source areas.

5.2.1. The upper member of the Huangliu Formation (8.2–5.5 Ma)

Zircon U–Pb data of the core sample in the upper member of the Huangliu Formation in the gas field yielded a wide range of crystallization ages (3169 ± 39 Ma to 83 ± 3 Ma), generally revealing a wide variety of sources. Zircon U–Pb ages form two major clusters at ca. 250 Ma and ca. 432 Ma, along with four subordinate clusters at ca. 757 Ma, ca. 1926 Ma, ca. 2529 Ma and ca. 2775 Ma (less than ±10% discordant) (Fig. 6A).

Indosinian zircon grains with an age peak at ca. 250 Ma are well developed in the Yangtze Block, the Hainan Uplift and the Truong

Son Belt, and are characterized by several large and small plutonic bodies (Fig. 9). Therefore, the age population probably relates to the collision between the Indochina and South China blocks and subsequent lateral extrusion of Indochina (Şengör et al., 1988; Lepvrier et al., 2008). The age ranges are ubiquitous and similar in these tectonic units, thus they are difficult to distinguish by U–Pb ages. Indosinian zircon grains extracted from sand of the modern Red River and granites in the southern Yangtze have a wide range of $\varepsilon_{Hf}(t)$ values of −20 to +15 with model ages between 2200 and 440 Ma (Hoang et al., 2009; Hiếu et al., 2013). The Permian I- and A-type granitoids associated with the Emeishan mantle plume in the Yangtze Block have relatively high positive $\varepsilon_{Hf}(t)$ values up to +14 (Xu et al., 2008; Shellnutt et al., 2009). Our unpublished data
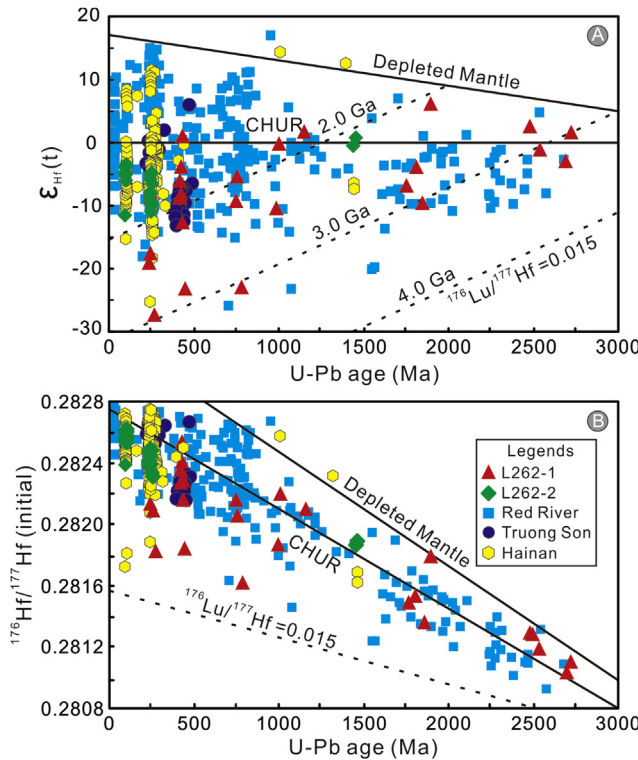
Figure 7. Plots of crystallization ages versus (A) ε_{Hf}(t), and (B) ^{176}Hf/^{177}Hf for all detrital zircon analyses from the two sedimentary rocks L262-1 and L262-2. CHUR: Chondritic Uniform Reservoir; dashed lines show the evolution of crustal volumes with ^{176}Hf/^{177}Hf = 0.015, corresponding to the average continental crust. Data of detrital zircons from the modern Red River and Red River Fault Zone are from Hoang et al. (2009) and Lin et al. (2012). Data for the Truong Son Belt are from our unpublished data. Data of the Mesozoic granites in the Hainan Island are from Wen (2013) and Wen et al. (2013).

Figure 8. Histograms of the two-stage Hf model ages for detrital zircons from the Huangliu Formation sandstones.

suggest that Permian zircon grains from the modern river on the eastern margin of the Indochina Block have ε_{Hf}(t) values ranging from −4.16 to +0.47 with model ages between 1200 and 840 Ma. A large number of Permian−Triassic zircons in the Hainan Uplift have ε_{Hf}(t) values between −10 and +1 with model ages concentrated between 1800 and 1200 Ma (Wen, 2013; Wen et al., 2013). The Indosinian ages in sample L262-1 gave ε_{Hf}(t) values at −27.91 to −7.76 (Fig. 7A) with model ages between 2438 and 1424 Ma (Fig. 8A), which are different from those of the Indosinian zircons in the Truong Son Belt, but similar to those of the Hainan and Red River in the southern Yangtze. The sediments of the Y-SH Basin are derived from several drainage systems, but the main input is the Red River (Song Hong) and its tributaries. The source of the Red River could be considered to be located mainly in the Yangtze Block (e.g. Hoang et al., 2009). Therefore, we suggest that the Indosinian zircon grains (ca. 250 Ma) were most likely derived from the southern Yangtze Block and the Hainan Uplift.

Caledonian zircon ages with an age peak at ca. 432 Ma are commonly related to the global tectonic-magmatic event termed the "Caledonian Orogeny", which is manifested by a number of Early Paleozoic magmatic and metamorphic rocks in East Asia (Lu et al., 1999). As discussed above, Ordovician and Silurian granitoids are well distributed in the southern Yangtze and Indochina blocks. A large area of plutonic intrusive rocks is exposed along the Red River Fault Zone and Truong Son Belt (Fig. 9). Despite the Caledonian zircon grains that have been detected from Hainan Island, they could account for only a small portion of the total amounts. The ε_{Hf}(t) values of these zircons range from −23.69 to +0.87 with model ages between 2378 and 1161 Ma, and mainly
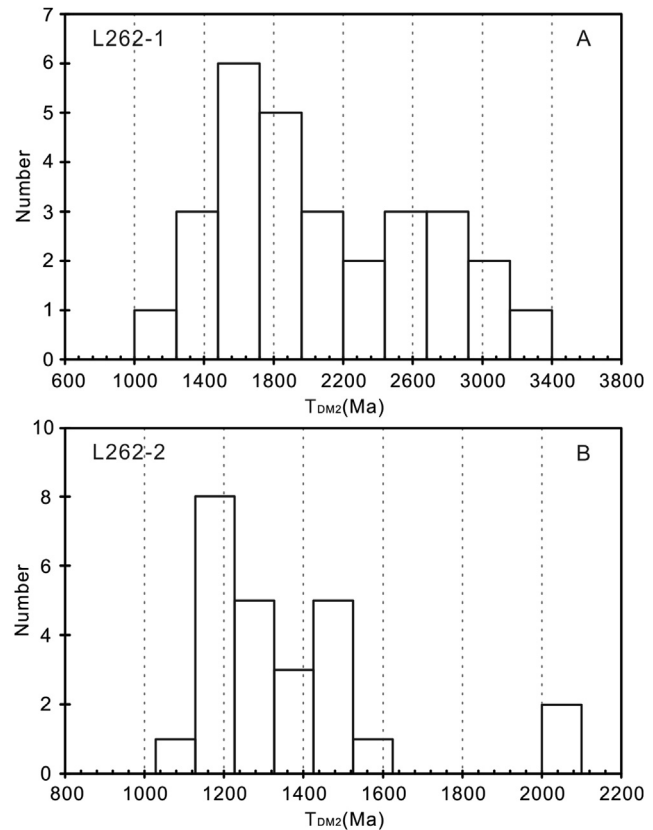
in a range of 1400−1200 Ma. Our unpublished data show that the Caledonian zircons from the modern river on the eastern margin of the Indochina Block have ε_{Hf}(t) values ranging from −12.71 to −6.34 with model ages between 1832 and 1549 Ma. The Caledonian zircon grains extracted from sand of the modern Red River have ε_{Hf}(t) values of −12.5 to +6.33 with model ages between 1602 and 883 Ma, with a peak at ca. 1200 Ma (Hoang et al., 2009). Although the ε_{Hf}(t) values have an intersection between the Indochina and Yangtze blocks, the model ages of the sample are closer to those of the Yangtze Block.

The Neoproterozoic ages with a peak at ca. 757 Ma (Fig. 6) are in response to the "Jinningian Movement (1000−700 Ma)" in the South China Block, and may be associated with the breakup of the Rodinian supercontinent (Li et al., 2002). Anorogenic granite intrusions are widely distributed in the Yangtze Block (Chen and Jahn, 1998) and range from mafic to felsic in composition (Lin et al., 2012). There are many rock outcrops along the Red River Fault Zone on the southern margin of the Yangtze Block, and their emplaced ages range from 840 to 740 Ma with a peak at ca. 810 Ma (Li et al., 2005, 2009; Wang et al., 2010) (Fig. 9). Neoproterozoic zircon grains have also been discovered in the Truong Son Belt with an age peak at ca. 958 Ma (Usuki et al., 2013), which is older than the ages obtained from our sample. Because mid-Neoproterozoic zircons have not been reported from Hainan Island, we infer that those zircons may have been derived from the southern Yangtze Block. The range of ages in our sample yielded ε_{Hf}(t) values of −23.72 to −0.38 with model ages between 2658 and 1692 Ma, suggesting that they were produced by reworking of Archean and Proterozoic crust.

Moreover, the Proterozoic (ca. 1926 Ma) and Archean age peaks (ca. 2775 Ma and 2529 Ma) in this sample (Fig. 6A) could be
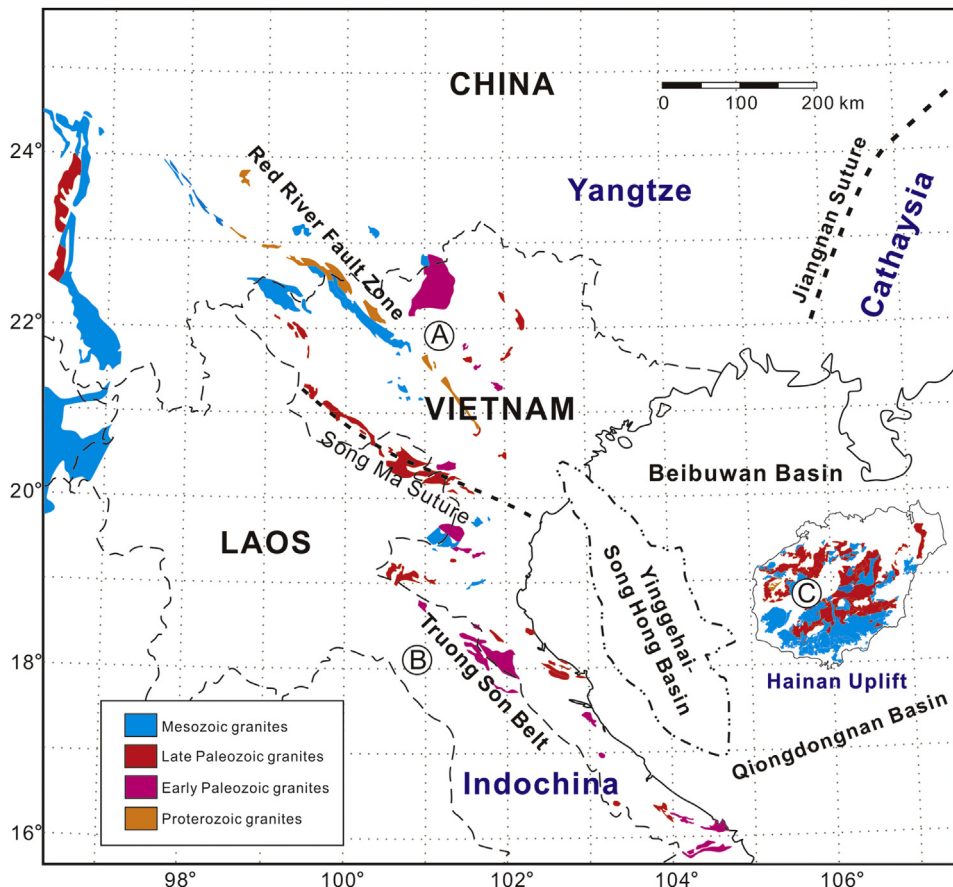
Figure 9. Distribution of the igneous rocks in the different tectonic units surrounding the Y-SH Basin.

considered to be sourced from the basement rocks of the Yangtze Block (Metcalfe, 2006).

Abundant detrital zircon grains in these age groups have rounded corners (Fig. 5), revealing long distance transport and/or sediment recycling. In addition, the age populations of the sample show a strong similarity to those of the upper Miocene sandstone in the Yen Bai Basin (Hoang et al., 2009), the major provenance of which was argued to be from the southern Yangtze Block through the paleo-Red River and its tributaries. This suggest that the upper member of the Huangliu Formation was mainly sourced from the southern Yangtze Block, and the Hainan Uplift also provided minor detritus to the basin at the same time.

5.2.2. The lower member of the Huangliu Formation (10.5–8.2 Ma)

Zircon grains from the lower member of the Huangliu Formation yield crystallization ages between 1457 and 93 Ma (Fig. 6B). U–Pb ages give two major age clusters at ca. 98 Ma and ca. 241 Ma, and a subordinate age cluster at ca. 1453 Ma (less than ±10% discordant) (Fig. 6B).

The Late Yanshanian zircon grains with a peak at ca. 98 Ma account for almost half of the total grains (45.9%), which coincides with those of the Cretaceous igneous rocks in Hainan Uplift (Fig. 9). The Yanshanian granites have been recognized in the southern Hainan and yielded ages range from 170 to 80 Ma (Wang et al., 1991, 2011; Jia et al., 2009; Yan et al., 2011). Detrital zircons from modern rivers in southern Hainan Island show a main age peak around 100 Ma (Wang et al., 2015), and may be interpreted as a signature of the Hainan Uplift because they are rare or absent in the other surrounding tectonic units. The $\varepsilon_{Hf}(t)$ values of these zircons range

from −11.57 to −4.98 with model ages between 1237 and 1095 Ma, revealing that they were derived from the Mesoproterozoic crust.

The Late Permian–Triassic zircon U–Pb ages with a peak at ca. 241 Ma are consistent with those of the Indosinian granites in the South China Block. Also, the Permian (272–254 Ma) and Triassic (249–227 Ma) granitoids (Wen et al., 2013) which are dominantly shoshonitic-high-K A-type and I-type granites (Li et al., 2006; Xie et al., 2006a; Wen et al., 2013) have been widely discovered in the Hainan Uplift. The Late Permian–Triassic zircons in our sample have negative $\varepsilon_{Hf}(t)$ values of −10.78 to −4.79 with the Meso-proterozoic model ages (Table 2), which are consistent with the $\varepsilon_{Hf}(t)$ values (−10 to +1) in the Hianan Uplift, suggesting they were largely derived from recycling of an old crust.

Two Mesoproterozoic zircon grains in the sample have $\varepsilon_{Hf}(t)$ values of −0.65 and +0.60 with model ages of 2073 and 2023 Ma. The two grains have older Hf mode ages than their U–Pb ages, suggesting some degree of reworking of existing crust in the magmatic episode (He et al., 2013). The Mesoproterozoic felsic volcanic rocks in the western Hainan Island were dated at 1460–1430 Ma, which was considered to be related to the Gren-villian orogeny in Asia (Xu et al., 2007; Li et al., 2008).

The detrital zircon grains in these age populations are mostly euhedral to subhedral in shape (Fig. 5), suggesting that the clastic materials were mostly derived from a local source. The general absence of Palaeozoic, Neoproterozoic and older zircon pop-ulations (>1500 Ma), but abundant Cretaceous ages implies that there were no clastic materials derived from the Yangtze Block and the Truong Son Belt. The lower member of the Huangliu Formation on the eastern margin was only derived from the Hainan Uplift.

In summary, the source areas for the lower and upper members of the Huangliu Formation are different in the Lingtou gas field (Drill L262). The provenance of the lower member was from the adjoining Hainan Uplift, east of the basin, whereas the sediment of the upper member was mainly derived from the southern Yangtze Block, northwest of the basin. The possible provenance directions and transport routes of the Upper Miocene Huangliu Formation are shown in Figure 10.

Combined with the age data from the Dongfang gas field (Wang et al., 2014) and Eastern Slope (Yan et al., 2007) of the basin, we suggest that the diversity of the age populations in the source areas reflect changes in sediment supply to the sample locations. In the central Y-SH Basin, the age populations are complicated with a wide range of zircon ages, which indicates multiple sources from the Yangtze Block, Hainan Island and Indochina Block (Wang et al., 2014). However, the age populations in the eastern Y-SH Basin are more simple, with two major age peaks consistent with derivation from Hainan Island (Yan et al., 2011). Compared with the provenance characteristics of the early and late stages of the Late Miocene (Fig. 10), we find that the source change happened only in the Lingtou gas field, which means the northwestern source (Red River) changed from short to long distance transport during the Late Miocene. The provenance change in this area may have been related to the tectonic event in East Asia.

5.3. Tectonic implication

The Y-SH Basin is a principal repository of the materials eroded by the Red River drainage and should be sensitive to changes in erosion rate in eastern Tibet. The U—Pb ages and Hf isotopes of the detrital zircons suggest a provenance change between the upper and lower members of the Huangliu Formation in the Lingtou gas field. The Late Miocene provenance change may be in response to a major phase of Tibetan Plateau uplift, an important tectonic event that affected a wide area in the South China and Indochina blocks during the Late Miocene (Liu and Yin, 2002).

The collision between India and Asia in southeastern Asia may have occurred before ca. 55 Ma (Lee and Lawver, 1995; Tapponnier et al., 2001), which set up a series of chain reactions and caused the uplift of the Tibetan Plateau in southeastern Asia (Molnar and Tapponnier, 1975, 1978; Tapponnier et al., 1986). The mechanism for the uplift of the Tibetan Plateau is still controversial, and the major hypotheses include the distributed shortening model

(England and Houseman, 1986; Molnar et al., 1993) and the continental extrusion model (Tapponnier et al., 1982, 2001). The provenance change is consistent with the broad climate change in the Late Miocene (Harrison et al., 1992; Molnar et al., 1993), which was affected significantly by increases in altitude of the plateau (An et al., 2001). Erosion patterns in southeastern Asia may have been related to rock uplift rates, but are presently not climatically controlled (Burbank et al., 2003; Hoang et al., 2009). Wan et al. (2007) used a multi-proxy approach to reconstruct the past change of the East Asian monsoon since 20 Ma. The results show that a profound shift occurred at ca. 8 Ma, which is in accordance with the time of the stratigraphic boundary between the upper and lower members of the Huangliu Formation (8.2 Ma). They also argued that the phased uplift of the Tibetan Plateau played a significant role in strengthening the Asian monsoon.

Additional studies also support this above conclusion. For example, Clift and Sun (2006) suggested that the sedimentation rates in the Y-SH Basin increased sharply at the end of the Miocene. Clark et al. (2005) used an initiation of the major river incisions to identify the timing of the initial uplift at 13—9 Ma and the high erosion rates between 0.23 and 0.47 mm/yr, and the result does coincide with the thermochronology data published by Xu and Kamp (2000) and Kirby et al. (2002). Gong and Li (2004) found that the uplift of the Tibetan Plateau since 10 Ma has had an important influence on the climate and sedimentary environment of the South China Sea, and the thick infill of the Y-SH Basin has been supplied by paleo-Red River delta during the Late Miocene.

The provenance evolution of the Y-SH Basin can be summarized as follows: on the eastern margin of the basin, owing to paleogeographic and climate frameworks, the Hainan Uplift as a local and single source provided detritus to the Huangliu Formation during the early stage of the Late Miocene (10.5—8.2 Ma). The uplift of the eastern Tibetan Plateau induced by the collision between India and Asia, instigated a climate change in southern Asia and hence an increase in erosion. The paleo-Red River would have been able to carry more detritus to greater distances, and thus the eastern side of the Y-SH Basin began to receive detritus from the southern Yangtze Block during the late stage of the Late Miocene (8.2—5.5 Ma) (Fig. 10).

6. Conclusions

The detrital zircon U—Pb ages and Hf isotopes show a marked difference between the upper and lower members of the Huangliu
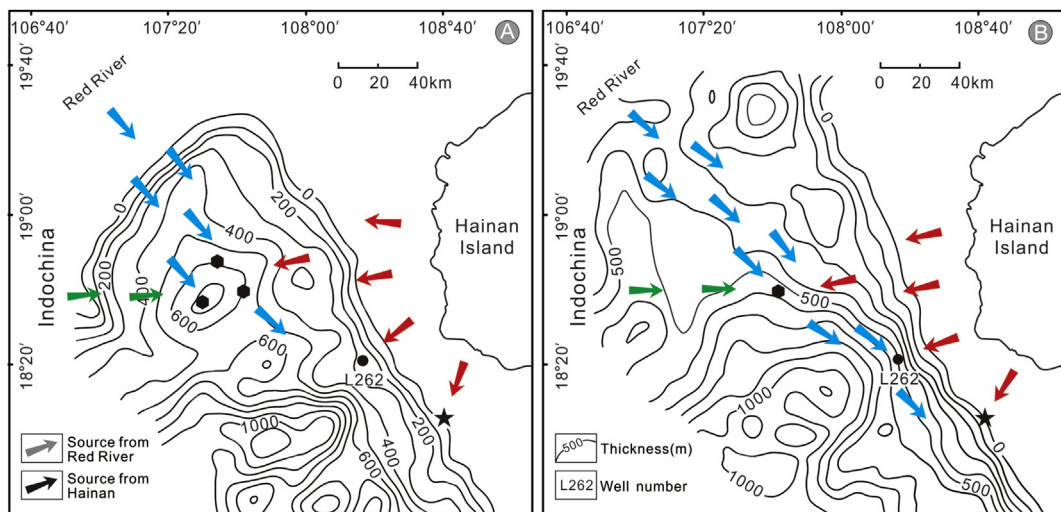
Figure 10. Possible provenance directions of the Upper Miocene Huangliu Formation on the eastern margin of the Y-SH Basin: (A) the early stage of the Late Miocene and (B) the late stage of the Late Miocene. The sediment isopach is modified after Gong et al. (1997). Symbols are as in Figure 1.

Formation in the Lingtou gas field, eastern margin of the Yinggehai-Song Hong Basin. The age spectra from the lower member are comparatively simple with two sharp and well-defined peaks. The $\varepsilon_{Hf}(t)$ values of the zircons are mostly negative, revealing that the zircons were largely derived from recycling of an old crust. The age spectra of the upper member are diverse with a wide range of ages and multiple peaks. The initial Hf isotope ratios [$\varepsilon_{Hf}(t)$] exhibit negative to positive values, suggesting that the existing crustal materials were mixing with new mantle melts. The diverse U—Pb ages and Hf isotope patterns suggest different source areas and changes in sediment supply to the sample locations. The provenance of the upper member was largely derived from the Yangtze Block, whereas detritus of the lower member was derived from the Hainan Uplift. The change in provenance provides an important clue in understanding the movement of the Tibetan Plateau and its influence on the South China Sea during the Late Miocene. According to the uplift history of the Tibetan Plateau and the climate and sedimentation rate changes on the northern margin of the South China Sea, the provenance change may correspond to a major phase of Tibetan Plateau uplift during the Late Miocene.

Acknowledgments

Appendix A. Supplementary data

Supplementary data related to this article can be found at http://dx.doi.org/10.1016/j.marpetgeo.2014.12.004.

References

An, Z., Kutzbach, J.E., Prell, W.L., Porter, S.C., 2001. Evolution of Asian monsoons and phased uplift of the Himalaya-Tibetan plateau since Late Miocene times. Nature 411, 62—66.

Andersen, T., 2002. Correction of common lead in U—Pb analyses that do not report [204]Pb. Chem. Geol. 192, 59—79.

Beltrán-Triviño, A., Winkler, W., Quadt, A., 2013. Tracing Alpine sediment sources through laser ablation U—Pb dating and Hf-isotopes of detrital zircons. Sedimentology 60, 197—224.

Black, L.P., Kamo, S.L., Allen, C.M., Aleinikoff, J.N., Davis, D.W., Korsch, R.J., Foudoulis, C., 2003. TEMORA 1: a new zircon standard for Phanerozoic U—Pb geochronology. Chem. Geol. 200, 155—170.

Blichert-Toft, J., Albarède, F., 1997. The Lu—Hf isotope geochemistry of chondrites and the evolution of the mantle-crust system. Earth Planet. Sci. Lett. 148, 243—258.

Burbank, D., Blythe, A., Putkonen, J., Pratt-Sitaula, B., Gabet, E., Oskin, M., Barros, A., Ojha, T., 2003. Decoupling of erosion and precipitation in the Himalayas. Nature 426, 652—655.

Carter, A., Roques, D., Bristow, C., Kinny, P., 2001. Understanding Mesozoic accretion in Southeast Asia: significance of Triassic thermotectonism (Indosinian orogeny) in Vietnam. Geology 29, 211—214.

Chen, J., Jahn, B.m, 1998. Crustal evolution of southeastern China: Nd and Sr isotopic evidence. Tectonophysics 284, 101—133.

Chen, Z., Lin, W., Faure, M., Lepvrier, C., Van Vuong, N., Van Tich, V., 2014. Geochronology and isotope analysis of the Late Paleozoic to Mesozoic granitoids from Northeastern Vietnam and implications for the evolution of the South China block. J. Asian Earth Sci. 86, 131—150.

Clark, M.K., House, M., Royden, L., Whipple, K., Burchfiel, B., Zhang, X., Tang, W., 2005. Late Cenozoic uplift of southeastern Tibet. Geology 33, 525—528.

Clift, P.D., Sun, Z., 2006. The sedimentary and tectonic evolution of the Yinggehai-Song Hong basin and the southern Hainan margin, South China Sea:

implications for Tibetan uplift and monsoon intensification. J. Geophys. Res. Solid Earth (1978—2012) 111, B06405. http://dx.doi.org/10.1029/2005JB004048.

England, P., Houseman, G., 1986. Finite strain calculations of continental deformation: 2. Comparison with the India-Asia collision zone. J. Geophys. Res. Solid Earth (1978—2012) 91, 3664—3676.

Geng, A., Zhou, Y., Fu, J., Sheng, G., Zhang, Q., 1998. The generation and expulsion of gases in Ya131 gas field, South China Sea: implication of laboratory pyrolysis results. J. Asian Earth Sci. 16, 429—436.

Gilley, L.D., Harrison, T.M., Leloup, P., Ryerson, F., Lovera, O.M., Wang, J., 2003. Direct dating of left-lateral deformation along the Red River shear zone, China and Vietnam. J. Geophys. Res. Solid Earth (1978—2012) 108 (B2), 2127. http://dx.doi.org/10.1029/2001JB001726.

Gong, Z., Li, S., 2004. Dynamic Research of Oil and Gas Accumulation in Northern Marginal Basins of South China Sea. Science Press, Beijing (in Chinese).

Gong, Z., Li, S., Xie, T., Zhang, Q., Xu, S., Xia, K., Yang, J., Sun, Y., Liu, L., 1997. Continental Margin Basin Analysis and Hydrocarbon Accumulation of the Northern South China Sea. Science Press, Beijing (in Chinese).

Griffin, W., Belousova, E., Shee, S., Pearson, N., O'reilly, S., 2004. Archean crustal evolution in the northern Yilgarn Craton: U—Pb and Hf-isotope evidence from detrital zircons. Precambrian Res. 131, 231—282.

Griffin, W., Pearson, N., Belousova, E., Jackson, S., Van Achterbergh, E., O'Reilly, S.Y., Shee, S., 2000. The Hf isotope composition of cratonic mantle: LAM-MC-ICPMS analysis of zircon megacrysts in kimberlites. Geochim. Cosmochim. Acta 64, 133—147.

Griffin, W., Wang, X., Jackson, S., Pearson, N., O'Reilly, S.Y., Xu, X., Zhou, X., 2002. Zircon chemistry and magma mixing, SE China: in-situ analysis of Hf isotopes, Tonglu and Pingtan igneous complexes. Lithos 61, 237—269.

Guo, L., Zhong, Z., Wang, L., Shi, Y., Li, H., Liu, S., 2001. Regional tectonic evolution around Yinggehai basin of South China Sea. Geol. J. China Univ. 7, 1—12 (in Chinese with English abstract).

Harrison, T.M., Copeland, P., Kidd, W., Yin, A., 1992. Raising tibet. Science 255, 1663—1670.

He, M., Zheng, H., Clift, P.D., 2013. Zircon U—Pb geochronology and Hf isotope data from the Yangtze River sands: implications for major magmatic events and crustal evolution in Central China. Chem. Geol. 360, 186—203.

Hiếu, P.T., Chen, F.k., Thủy, N.T.B., Cư'ờng, N.Q., Li, S.Q., 2013. Geochemistry and zircon U—Pb ages and Hf isotopic composition of Permian alkali granitoids of the Phan Si Pan zone in northwestern Vietnam. J. Geodyn. 69, 106—121.

Hoa, T.T., Izokh, A., Polyakov, G., Borisenko, A., Anh, T.T., Balykin, P., Phuong, N.T., Rudnev, S., Van, V.V., Nien, B.A., 2008. Permo-Triassic magmatism and metallogeny of Northern Vietnam in relation to the Emeishan plume. Russ. Geol. Geophys. 49, 480—491.

Hoang, L.V., Wu, F., Clift, P.D., Wysocka, A., Swierczewska, A., 2009. Evaluating the evolution of the Red River system based on in situ U—Pb dating and Hf isotope analysis of zircons. Geochem. Geophys. Geosyst. 10, Q11008. http://dx.doi.org/10.1029/2009GC002819.

Huang, B., Xiao, X., Hu, Z., Yi, P., 2005. Geochemistry and episodic accumulation of natural gases in the Ledong gas field in the Yinggehai Basin, offshore South China Sea. Org. Geochem. 36, 1689—1702.

Huang, B., Xiao, X., Li, X., 2003. Geochemistry and origins of natural gases in the Yinggehai and Qiongdongnan basins, offshore South China Sea. Org. Geochem. 34, 1009—1025.

Huang, B., Xiao, X., Li, X., Cai, D., 2009. Spatial distribution and geochemistry of the nearshore gas seepages and their implications to natural gas migration in the Yinggehai Basin, offshore South China Sea. Mar. Pet. Geol. 26, 928—935.

Huang, X., Xu, Y., Lan, J., Yang, Q., Luo, Z., 2009. Neoproterozoic adakitic rocks from Mopanshan in the western Yangtze Craton: Partial melts of a thickened lower crust. Lithos 112, 367—381.

Jackson, S.E., Pearson, N.J., Griffin, W.L., Belousova, E.A., 2004. The application of laser ablation-inductively coupled plasma-mass spectrometry to in situ U—Pb zircon geochronology. Chem. Geol. 211, 47—69.

Jia, X., Wang, Q., Tang, G., Jiang, Z., Zhao, Z., Yang, Y., Wang, X., ZHao, W., 2009. Zircon U—Pb geochronology, geochemistry and petrogenesis of the Late Early Cretaceous adakitic intrusive rocks in the Tunchang area, Hainan Province. Geochimica 39, 497—519 (in Chinese with English abstract).

Kirby, E., Reiners, P.W., Krol, M.A., Whipple, K.X., Hodges, K.V., Farley, K.A., Tang, W., Chen, Z., 2002. Late Cenozoic evolution of the eastern margin of the Tibetan Plateau: inferences from [40]Ar/[39]Ar and (U—Th)/He thermochronology. Tectonics 21. http://dx.doi.org/10.1029/2000TC001246.

Lan, C.Y., Chung, S.L., Van Long, T., Lo, C.H., Lee, T.Y., Mertzman, S.A., Jiun-San Shen, J., 2003. Geochemical and Sr—Nd isotopic constraints from the Kontum massif, central Vietnam on the crustal evolution of the Indochina block. Precambrian Res. 122, 7—27.

Lee, T.Y., Lawver, L.A., 1995. Cenozoic plate reconstruction of Southeast Asia. Tectonophysics 251, 85—138.

Lei, C., Ren, J., Clift, P.D., Wang, Z., Li, X., Tong, C., 2011. The structure and formation of diapirs in the Yinggehai-Song Hong Basin, South China Sea. Mar. Pet. Geol. 28, 980—991.

Leloup, P.H., Lacassin, R., Tapponnier, P., Schärer, U., Zhong, D., Liu, X., Zhang, L., Ji, S., Trinh, P.T., 1995. The Ailao Shan-Red River shear zone (Yunnan, China), tertiary transform boundary of Indochina. Tectonophysics 251, 3—84.

Lepvrier, C., Van Vuong, N., Maluski, H., Truong Thi, P., Van Vu, T., 2008. Indosinian tectonics in Vietnam. C. R. Geosci. 340, 94—111.

Li, W., Li, X., Li, Z., 2005. Neoproterozoic bimodal magmatism in the Cathaysia Block of South China and its tectonic significance. Precambrian Res. 136, 51—66.

Li, X., Li, W., Li, Z., Lo, C., Wang, J., Ye, M., Yang, Y., 2009. Amalgamation between the Yangtze and Cathaysia Blocks in South China: constraints from SHRIMP U–Pb zircon ages, geochemistry and Nd–Hf isotopes of the Shuangxiwu volcanic rocks. Precambrian Res. 174, 117–128.

Li, X., Li, Z., Li, W., Wang, Y., 2006. Initiation of the Indosinian Orogeny in South China: evidence for a Permian magmatic arc on Hainan Island. J. Geol. 114, 341–353.

Li, X., Long, W., Li, Q., Liu, Y., Zheng, Y., Yang, Y., Chamberlain, K.R., Wan, D., Guo, C., Wang, X., 2010. Penglai zircon megacrysts: a potential new working reference material for microbeam determination of Hf–O isotopes and U–Pb age. Geostand. Geoanal. Res. 34, 117–134.

Li, Z., Li, X., Kinny, P., Wang, J., Zhang, S., Zhou, H., 2003. Geochronology of Neoproterozoic syn-rift magmatism in the Yangtze Craton, South China and correlations with other continents: evidence for a mantle superplume that broke up Rodinia. Precambrian Res. 122, 85–109.

Li, Z., Li, X., Li, W., Ding, S., 2008. Was Cathaysia part of Proterozoic Laurentia?-new data from Hainan Island, south China. Terra Nova 20, 154–164.

Li, Z., Li, X., Zhou, H., Kinny, P.D., 2002. Grenvillian continental collision in south China: new SHRIMP U–Pb zircon results and implications for the configuration of Rodinia. Geology 30, 163–166.

Lin, T., Chung, S., Chiu, H., Wu, F., Yeh, M., Searle, M.P., Iizuka, Y., 2012. Zircon U–Pb and Hf isotope constraints from the Ailao Shan-Red River shear zone on the tectonic and crustal evolution of southwestern China. Chem. Geol. 291, 23–37.

Ling, W., Gao, S., Zhang, B., Li, H., Liu, Y., Cheng, J., 2003. Neoproterozoic tectonic evolution of the northwestern Yangtze craton, South China: implications for amalgamation and break-up of the Rodinia Supercontinent. Precambrian Res. 122, 111–140.

Liu, J., Tran, M.D., Tang, Y., Nguyen, Q.L., Tran, T.H., Wu, W., Chen, J., Zhang, Z., Zhao, Z., 2012. Permo-Triassic granitoids in the northern part of the Truong Son belt, NW Vietnam: geochronology, geochemistry and tectonic implications. Gondwana Res. 22, 628–644.

Liu, X., Yin, Z., 2002. Sensitivity of East Asian monsoon climate to the uplift of the Tibetan Plateau. Palaeogeogr. Palaeoclimatol. Palaeoecol. 183, 223–245.

Liu, Y., Gao, S., Hu, Z., Gao, C., Zong, K., Wang, D., 2010. Continental and oceanic crust recycling-induced melt-peridotite interactions in the trans-north China Orogen: U–Pb dating, Hf isotopes and trace elements in Zircons from Mantle Xenoliths. J. Petrol. 51, 537–571.

Liu, Y., Hu, Z., Gao, S., Günther, D., Xu, J., Gao, C., Chen, H., 2008. In situ analysis of major and trace elements of anhydrous minerals by LA-ICP-MS without applying an internal standard. Chem. Geol. 257, 34–43.

Lu, S., Li, H., Yu, H., Zhao, F., Yang, C., 1999. Neoproterozoic orogeny in northwestern China. Gondwana Res. 2, 610–611.

Ludwig, K.R., 2003. User's Manual for Isoplot 3.00: a Geochronological Toolkit for Microsoft Excel. Kenneth R. Ludwig.

Luo, X., Dong, W., Yang, J., Yang, W., 2003. Overpressuring mechanisms in the Yinggehai basin, south China Sea. AAPG Bull. 87, 629–645.

Meinhold, G., Reischmann, T., Kostopoulos, D., Lehnert, O., Matukov, D., Sergeev, S., 2008. Provenance of sediments during subduction of Palaeotethys: detrital zircon ages and olistolith analysis in Palaeozoic sediments from Chios Island, Greece. Palaeogeogr. Palaeoclimatol. Palaeoecol. 263, 71–91.

Metcalfe, I., 2006. Palaeozoic and Mesozoic tectonic evolution and palaeogeography of East Asian crustal fragments: the Korean Peninsula in context. Gondwana Res. 9, 24–46.

Molnar, P., England, P., Martinod, J., 1993. Mantle dynamics, uplift of the Tibetan Plateau, and the Indian monsoon. Rev. Geophys. 31, 357–396.

Molnar, P., Tapponnier, P., 1975. Cenozoic tectonics of Asia: effects of a continental collision. Science 189, 419–426.

Molnar, P., Tapponnier, P., 1978. Active tectonics of Tibet. J. Geophys. Res. Solid Earth (1978–2012) 83, 5361–5375.

Morton, A., Claoué-Long, J., Hallsworth, C., 2001. Zircon age and heavy mineral constraints on provenance of North Sea Carboniferous sandstones. Mar. Pet. Geol. 18, 319–337.

Roger, F., Leloup, P.H., Jolivet, M., Lacassin, R., Trinh, P.T., Brunel, M., Seward, D., 2000. Long and complex thermal history of the Song Chay metamorphic dome (Northern Vietnam) by multi-system geochronology. Tectonophysics 321, 449–466.

Roger, F., Maluski, H., Lepvrier, C., Vu Van, T., Paquette, J.L., 2012. LA-ICPMS zircons U/Pb dating of Permo-Triassic and Cretaceous magmatisms in Northern Vietnam-Geodynamical implications. J. Asian Earth Sci. 48, 72–82.

Scherer, E., Münker, C., Mezger, K., 2001. Calibration of the lutetium-hafnium clock. Science 293, 683–687.

Şengör, A., Altıner, D., Cin, A., Ustaömer, T., Hsü, K., 1988. Origin and Assembly of the Tethyside Orogenic Collage at the Expense of Gondwana Land. In: Geological Society, London, Special Publications 37, pp. 119–181.

Shellnutt, J.G., Wang, C.Y., Zhou, M., Yang, Y., 2009. Zircon Lu–Hf isotopic compositions of metaluminous and peralkaline A-type granitic plutons of the Emeishan large igneous province (SW China): constraints on the mantle source. J. Asian Earth Sci. 35, 45–55.

Sun, Z., Zhou, D., Zhong, Z., Zeng, Z., Wu, S., 2003. Experimental evidence for the dynamics of the formation of the Yinggehai basin, NW South China Sea. Tectonophysics 372, 41–58.

Tapponnier, P., Lacassin, R., Leloup, P.H., Schärer, U., Zhong, D., Wu, H., Liu, X., Ji, S., Zhang, L., Zhong, J., 1990. The Ailao Shan/Red River metamorphic belt: tertiary left-lateral shear between Indochina and South China. Nature 343, 431–437.

Tapponnier, P., Peltzer, G., Armijo, R., 1986. On the Mechanics of the Collision between India and Asia. In: Geological Society, London, Special Publications 19, pp. 113–157.

Tapponnier, P., Peltzer, G., Le Dain, A., Armijo, R., Cobbold, P., 1982. Propagating extrusion tectonics in Asia: new insights from simple experiments with plasticine. Geology 10, 611–616.

Tapponnier, P., Xu, Z., Roger, F., Meyer, B., Arnaud, N., Wittlinger, G., Yang, J., 2001. Oblique stepwise rise and growth of the Tibet Plateau. science 294, 1671–1677.

Tsikouras, B., Pe-Piper, G., Piper, D.J., Schaffer, M., 2011. Varietal heavy mineral analysis of sediment provenance, Lower Cretaceous Scotian Basin, eastern Canada. Sediment. Geol. 237, 150–165.

Usuki, T., Lan, C.Y., Wang, K.L., Chiu, H.Y., 2013. Linking the Indochina block and Gondwana during the Early Paleozoic: evidence from U–Pb ages and Hf isotopes of detrital zircons. Tectonophysics 586, 145–159.

Usuki, T., Lan, C.-Y., Yui, T.-F., Iizuka, Y., Van Vu, T., Tran, T.A., Okamoto, K., Wooden, J.L., Liou, J.G., 2009. Early Paleozoic medium-pressure metamorphism in central Vietnam: evidence from SHRIMP U–Pb zircon ages. Geosci. J. 13, 245–256.

Wan, S., Li, A., Clift, P.D., Stuut, J.-B.W., 2007. Development of the East Asian monsoon: mineralogical and sedimentologic records in the northern South China Sea since 20 Ma. Palaeogeogr. Palaeoclimatol. Palaeoecol. 254, 561–582.

Wang, C., Liang, X., Xie, Y., Tong, C., Pei, J., Zhou, Y., Jiang, Y., Fu, J., Liu, P., 2014. Provenance of Upper Miocene to Quaternary sediments in the Yinggehai-Song Hong Basin, South China Sea: evidence from detrital zircon U–Pb ages. Mar. Geol. 355, 202–217.

Wang, C., Liang, X.Q., Zhou, Y., Jiang, Y., Fu, J., Jiang, Y., Dong, C., Tong, C., Pei, J., Liu, P., 2015. Construction of age frequences of provenances on the eastern side of the Yinggehai Basin: studies on LA-ICP-MS U-Pb ages of detrital zircons from six modern rivers, Western Hainan, China. Earth Sci. Front. 22 (in press) (in Chinese with English abstract).

Wang, Q., Wyman, D.A., Li, Z., Bao, Z., Zhao, Z., Wang, Y., Jian, P., Yang, Y., Chen, L., 2010. Petrology, geochronology and geochemistry of ca. 780 Ma A-type granites in South China: petrogenesis and implications for crustal growth during the breakup of the supercontinent Rodinia. Precambrian Res. 178, 185–208.

Wang, X., Ma, D., Jiang, D., 1991. Geology in Hainan Island. Geological Publishing House, Beijing (in Chinese).

Wang, Z., Huang, B., 2008. Dongfang 1-1 gas field in the mud diapir belt of the Yinggehai Basin, South China Sea. Mar. Pet. Geol. 25, 445–455.

Wang, Z., Xu, D., Zhang, Y., Chen, F., Wang, L., Wu, J., 2011. Zircon LA-ICP-MS U–Pb dating of the granodiorite Porphyry from the Shilu Iron Ore Deposit, Hainan Province and its geological implications. Geotect. Metallog. 35, 292–299 (in Chinese with English abstract).

Wen, S., 2013. Geochronologic and Geochemical Studies of Permian-Triassic Magmatism in Hainan Island, South China (PhD dissertation). University of Chinese Academy of Sciences (in Chinese with English abstract).

Wen, S., Liang, X., Fan, W., Wang, Y., Chi, G., Liang, x., Zhou, Y., Jiang, Y., 2013. Zircon U–Pb ages, Hf isotopic composition of Zhizhong granitic intrusion in Ledong Area of Hainan Island and their tectonic implications. Geotect. Metallog. 37, 294–307 (in Chinese with English abstract).

Wu, F., 1997. Discussion on the formation conditions of Gas Reservoirs in Yinggehai Basin. Nat. Gas Ind. 17, 6–10 (in Chinese with English abstract).

Wu, F., Ji, W., Liu, C., Chung, S., 2010. Detrital zircon U–Pb and Hf isotopic data from the Xigaze fore-arc basin: constraints on Transhimalayan magmatic evolution in southern Tibet. Chem. Geol. 271, 13–25.

Wu, F., Yang, Y., Xie, L., Yang, J., Xu, P., 2006. Hf isotopic compositions of the standard zircons and baddeleyites used in U–Pb geochronology. Chem. Geol. 234, 105–126.

Wu, Y., Zheng, Y., 2004. Genesis of zircon and its constraints on interpretation of U–Pb age. Chin. Sci. Bull. 49, 1554–1569.

Xie, C., Zhu, J., Ding, S., Zhang, Y., Chen, M., Fu, Y., Fu, T., Li, Z., 2006a. Age and petrogenesis of the Jianfengling granite and its relationship to metallogenesis of the Baolun gold deposite, Hainan Island. Acta Petrol. Sin. 22, 2493–2508 (in Chinese with English abstract).

Xie, C., Zhu, J., Ding, S., Zhang, Y., Li, Z., 2006b. Identification of Hercynian shoshonitic intrusive rocks in central Hainan Island and its geotectonic implications. Chin. Sci. Bull. 51, 2507–2519 (in Chinese with English abstract).

Xie, X., Li, S., Dong, W., Hu, Z., 2001. Evidence for episodic expulsion of hot fluids along faults near diapiric structures of the Yinggehai Basin, South China Sea. Mar. Pet. Geol. 18, 715–728.

Xie, Y., 2009. Sequence Stratigraphic Analysis and Hydrocarbon Accumulation Models in Tectonically Active Basins-case Study on the Yinggehai Basin. Geological Publishing House, Beijing (in Chinese with English abstract).

Xu, D., Xia, B., Li, P., Chen, G., Ma, C., Zhang, Y., 2007. Protolith natures and U–Pb sensitive high mass-resolution ion microprobe (SHRIMP) zircon ages of the metabasites in Hainan Island, South China: Implications for geodynamic evolution since the late Precambrian. Isl. Arc 16, 575–597.

Xu, G., Kamp, P.J., 2000. Tectonics and denudation adjacent to the Xianshuihe Fault, eastern Tibetan Plateau: constraints from fission track thermochronology. J. Geophys. Res. Solid Earth (1978–2012) 105, 19231–19251.

Xu, Y., Luo, Z., Huang, X., He, B., Xiao, L., Xie, L., Shi, Y., 2008. Zircon U–Pb and Hf isotope constraints on crustal melting associated with the Emeishan mantle plume. Geochim. Cosmochim. Acta 72, 3084–3104.

Yan, D., Zhou, M., Wang, C.Y., Xia, B., 2006. Structural and geochronological constraints on the tectonic evolution of the Dulong-Song Chay tectonic dome in Yunnan province, SW China. J. Asian Earth Sci. 28, 332–353.

Yan, Y., Xia, B., Lin, G., Carter, A., Hu, X., Cui, X., Liu, B., Yan, P., Song, Z., 2007. Geochemical and Nd isotope composition of detrital sediments on the north margin of the South China Sea: provenance and tectonic implications. Sedimentology 54, 1–17.

Yan, Y., Carter, A., Palk, C., Brichau, S., Hu, X., 2011. Understanding sedimentation in the Song Hong-Yinggehai Basin, South China Sea. Geochem. Geophys. Geosyst. 12, Q06014. http://dx.doi.org/10.1029/2011GC003533.

Yang, D., Xu, W., Xu, Y., Wang, Q., Pei, F., Wang, F., 2012a. U—Pb ages and Hf isotope data from detrital zircons in the Neoproterozoic sandstones of northern Jiangsu and southern Liaoning Provinces, China: implications for the Late Precambrian evolution of the southeastern North China Craton. Precambrian Res. 216, 162—176.

Yang, J., Cawood, P.A., Du, Y., Huang, H., Huang, H., Tao, P., 2012b. Large Igneous Province and magmatic arc sourced Permian—Triassic volcanogenic sediments in China. Sediment. Geol. 261, 120—131.

Yuan, H., Gao, S., Dai, M., Zong, C., Günther, D., Fontaine, G.H., Liu, X., Diwu, C., 2008. Simultaneous determinations of U—Pb age, Hf isotopes and trace element compositions of zircon by excimer laser-ablation quadrupole and multiple-collector ICP-MS. Chem. Geol. 247, 100—118.

Yuan, H., Gao, S., Liu, X., Li, H., Günther, D., Wu, F., 2004. Accurate U—Pb age and trace element determinations of zircon by laser ablation-inductively coupled plasma-mass spectrometry. Geostand. Geoanal. Res. 28, 353—370.

Zhang, H., Pei, J., Zhang, Y., 2013. Overpressure reservoirs in the mid-deep Huangliu Formation of the Dongfang area, Yinggehai Basin, South China Sea. Pet. Explor. Dev. 40, 284—293.

Zhang, Q., Liu, F., Yang, J., 1996. Overpressure system and hydrocarbon accumulation in the Yinggehai basin. China Offshore Oil Gas (Geol.) 10, 65—75 (in Chinese with English abstract).

Zhao, B., Wang, C., Wang, X., Feng, Z., 2013. Late Cretaceous (Campanian) provenance change in the Songliao Basin, NE China: evidence from detrital zircon U—Pb ages from the Yaojia and Nenjiang Formations. Palaeogeogr. Palaeoclimatol. Palaeoecol. 385, 83—94.

Zheng, J., Griffin, W., O'Reilly, S.Y., Zhang, M., Pearson, N., Pan, Y., 2006. Widespread Archean basement beneath the Yangtze craton. Geology 34, 417—420.

Zhong, H., Xu, G., Zhu, W., Hu, R., He, D., 2009. Petrogenesis of the Taihe Granite s in the Emeishan Large Igneous Province and its tectonic implications. Bulletin of Mineralogy. Petrol. Geochem. 29, 99—110 (in Chinese with English abstract).

Zhong, Y., Xu, Y., 2009. Characteristics of plume-related A-type granites: an example from Emeishan Large Igneous Province. J. Jilin Univ. (Earth Sci. Ed.) 39, 828—838 (in Chinese with English abstract).

Zhu, M., Graham, S., McHargue, T., 2009. The Red River fault zone in the Yinggehai Basin, South China Sea. Tectonophysics 476, 397—417.